AD-A084 176 DAVID W TAYLOR NAVAL SHIP RESEARCH AND DEVELOPMENT CE--ETC F/G 20/4
THE LOW-SPEED CHARACTERISTICS OF A 15-PERCENT QUASI-ELLIPTICAL --ETC(U)
MAY 79 J ABRAMSON
UNCLASSIFIED DTNSRDC/ASED-79/07 NL

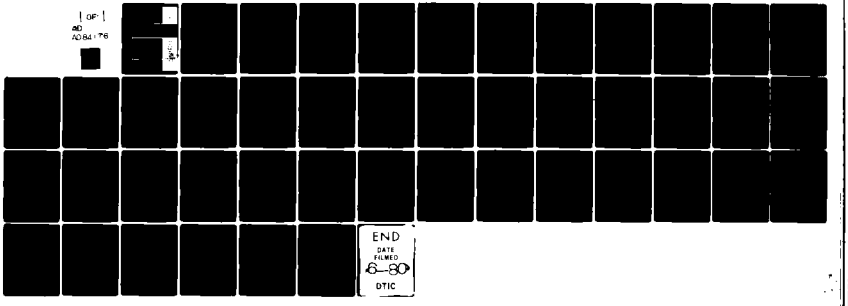

LEVEL II

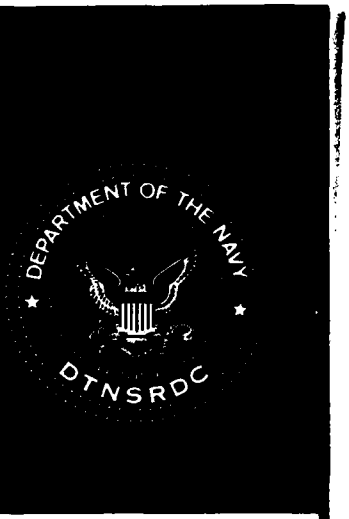

THE LOW-SPEED CHARACTERISTICS OF A 15-PERCENT QUASI-ELLIPTICAL CIRCULATION CONTROL AIRFOIL WITH DISTRIBUTED CAMBER

by

Jane Abramson

APPROVED FOR PUBLIC RELEASE:
DISTRIBUTION UNLIMITED

AVIATION AND SURFACE EFFECTS DEPARTMENT

DTNSRDC/ASED-79/07

May 1979

DAVID
W.
TAYLOR
NAVAL
SHIP
RESEARCH
AND
DEVELOPMENT
CENTER

BETHESDA
MARYLAND
20084

UNCLASSIFIED

SECURITY CLASSIFICATION OF THIS PAGE (When Data Entered)

REPORT DOCUMENTATION PAGE

READ INSTRUCTIONS BEFORE COMPLETING FORM

1. REPORT NUMBER: DTNSRDC/ASED-79/07	2. GOVT ACCESSION NO.: AD-A084 176
3. RECIPIENT'S CATALOG NUMBER:	
4. TITLE (and Subtitle): THE LOW-SPEED CHARACTERISTICS OF A 15-PERCENT QUASI-ELLIPTICAL CIRCULATION CONTROL AIRFOIL WITH DISTRIBUTED CAMBER	5. TYPE OF REPORT & PERIOD COVERED: Final
	6. PERFORMING ORG. REPORT NUMBER:
7. AUTHOR(s): Jane Abramson	8. CONTRACT OR GRANT NUMBER(s): 46
9. PERFORMING ORGANIZATION NAME AND ADDRESS: David W. Taylor Naval Ship R&D Center, Aviation and Surface Effects Department, Bethesda, Maryland 20084	10. PROGRAM ELEMENT, PROJECT, TASK AREA & WORK UNIT NUMBERS: Project Element 63203N, Task Area W0578, Work Unit 1619-300
11. CONTROLLING OFFICE NAME AND ADDRESS: Naval Air Systems Command, AIR-320D, Washington, D.C. 20361	12. REPORT DATE: May 1979
	13. NUMBER OF PAGES: 46
14. MONITORING AGENCY NAME & ADDRESS(if different from Controlling Office)	15. SECURITY CLASS. (of this report): UNCLASSIFIED
	15a. DECLASSIFICATION/DOWNGRADING SCHEDULE

16. DISTRIBUTION STATEMENT (of this Report)

APPROVED FOR PUBLIC RELEASE: DISTRIBUTION UNLIMITED

17. DISTRIBUTION STATEMENT (of the abstract entered in Block 20, if different from Report)

18. SUPPLEMENTARY NOTES

19. KEY WORDS (Continue on reverse side if necessary and identify by block number)

Two-Dimensional Wind Tunnel Testing
Circulation Control Airfoils
Elliptic Airfoil Sections
Tangential Blowing
Boundary Layer Control

20. ABSTRACT (Continue on reverse side if necessary and identify by block number)

The aerodynamic characteristics of a circulation control elliptic airfoil section with a 15-percent thickness-to-chord ratio were evaluated subsonically. The airfoil, designated NCCR1513-7559E, incorporates a high degree of nose camber and an increased leading edge radius in a profile designed for high subsonic speeds. Critical Mach numbers in excess of 0.7 were predicted analytically for several typical operating

(Continued on reverse side)

DD FORM 1 JAN 73 1473 EDITION OF 1 NOV 65 IS OBSOLETE
S/N 0102-014-6601

UNCLASSIFIED

SECURITY CLASSIFICATION OF THIS PAGE (When Data Entered)

(Block 20 continued)

conditions. Lift coefficients up to 4.63 were produced at momentum coefficients of 0.22. Equivalent lift-to-drag ratios of approximately 40 were also produced at $C_{(\ell)} = 0.8$.

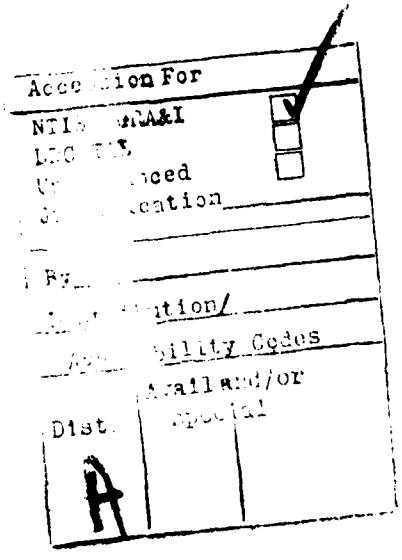

TABLE OF CONTENTS

LIST OF FIGURES

Page

LIST OF TABLES

NOTATION

a_j	Sonic velocity in the jet, ft/sec (m/s)
C_d	Sectional profile drag coefficient from momentum loss in wake, corrected for additional mass efflux of the jet
$C_{d_{rake}}$	Section profile drag coefficient as measured by rake, uncorrected
C_{d_e}	Equivalent drag coefficient, $C_d + C_\mu(V_j/2V_\infty) + C_\mu \frac{V_\infty}{V_j}$
C_ℓ	Sectional lift coefficient
$C_{\ell_{max}}$	Maximum sectional lift coefficient obtainable within test C_μ limitations
$C_{m_{50}}$	Pitching moment coefficient about the half-chord
C_p	Pressure coefficient, $(P_\ell - P_\infty)/q_\infty$
C_μ	Momentum coefficient, $\dot{m}V_j/(q_\infty S)$
c	Chord length, ft (m)
d	Profile drag corrected for jet mass efflux, lb (kg)
d_e	Equivalent drag, lb (N), $d + \dot{m}V_j^2/(2V_\infty)$
h	Slot height, in. (cm)
ℓ	Sectional lift, lb (kg)
ℓ/d_e	Equivalent section lift-to-drag ratio
M_{crit}	Critical Mach number
M_j	Mach number in the jet
$\dot{m}$	Mass efflux, slugs/sec
P_ℓ	Local static pressure on the model, lb/ft^2 (N/m^2)
P_t	Duct (plenum) total pressure, lb/ft^2 (N/m^2)
P_{t_∞}	Free-stream total pressure, lb/ft^2 (N/m^2)
P_∞	Free-stream static pressure, lb/ft^2 (N/m^2)
q_∞	Free-stream dynamic pressure, lb/ft^2 (N/m^2)
R	Universal gas constant

R_e	Reynolds number based on chord
S	Model planform area, ft^2 (m^2)
T_j	Jet static temperature, °R
T_t	Duct (plenum) total temperature, °R
t	Airfoil Thickness, ft (m)
V_j	Jet velocity, ft/sec (m/s)
V_∞	Free-stream velocity, ft/sec (m/s)
x	Chordwise distance from leading edge, ft (m)
x_s	Chordwise distance of the slot from leading edge, ft (m)
x/c	Dimensionless chordwise position
α	Geometric angle of attack, deg
γ	Ratio of specific heats

ABSTRACT

The aerodynamic characteristics of a circulation control elliptic airfoil section with a 15-percent thickness-to-chord ratio were evaluated subsonically. The airfoil, designated NCCR1513-7559E, incorporates a high degree of nose camber and an increased leading edge radius in a profile designed for high subsonic speeds. Critical Mach numbers in excess of 0.7 were predicted analytically for several typical operating conditions. Lift coefficients up to 4.63 were produced at momentum coefficients of 0.22. Equivalent lift-to-drag ratios of approximately 40 were also produced at $C_\ell \simeq 0.8$.

ADMINISTRATIVE INFORMATION

The work presented herein was conducted at the David W. Taylor Naval Ship Research and Development Center (DTNSRDC) for the Naval Air Systems Command (AIR-320D) under Project Element 6323N and Task Area WO578.

All data recorded during this experiment were either measured in or converted directly to U.S. customary units. Hence, U.S. customary units are the primary units in this report. Metric units are given adjacent to the U.S. units in parentheses. Angular measurement is the only exception; the unit of degrees is not converted to radians.

INTRODUCTION

Tangential blowing over the bluff trailing edge of a 15-percent cambered elliptic airfoil section was investigated experimentally. This airfoil is one of a series of five being evaluated in the circulation control airfoil development program at DTNSRDC to ascertain the effects of leading and trailing edge geometry on performance.[1,2*] All of the models employ the Coanda effect to obtain high-lift augmentation by tangentially ejecting a sheet of air near the trailing edge on the upper

*A complete listing of references is given on page 13.

surface. Because of the Coanda effect, the jet sheet remains attached to the bluff trailing edge and provides a mechanism for boundary layer control. The Coanda blowing can be thought of as a movement of the stagnation points thereby producing an increase in circulation.

MODEL AND TEST APPARATUS

The airfoil profile NCCR1513-7559E (see Table 1) was designed to operate at high subsonic speeds without unduly compromising low-speed augmentation characteristics. A further objective of the design was a reduction in the airfoil pitching moment about the 50-percent chord point. To accomplish these objectives a redefined ellipse with a 15-percent thickness-to-chord ratio and a 1.3-percent camber, as described by Wilkerson,[1] was:

> "modified to produce larger radii at both the leading edge, $(r/c)_{le} = 0.015$, and the trailing edge, $(r/c)_{te} = 0.020$. The trailing edge surface was obtained by modified thickness distribution, rather than the use of an inserted circular shape, in order to preserve compatibility between the upper surface slot and the trailing edge Coanda surface. The trailing edge is therefore a modified elliptical contour."

The model has a chord length of 8 in. (0.203 m) with an upper surface slot 7.8 in. (0.198 m) from the leading edge yielding a slot position x/c = 0.975-percent chord. Table 2 is a partial listing of the coordinates specified for model construction.

The outer shell of the model is constructed of wood with an internal steel plenum chamber through which air for the Coanda jet was introduced. The slot exit is the throat of a converging nozzle formed by the internal geometry of the Coanda surface and the underside of a knife-edged aluminum blade. The slot height was adjusted through the use of pitch screws. An undercut was made in the blade to ensure that the flow would exit tangentially to the model surface; see Figure 1.

The two-dimensional tests were conducted at DTNSRDC in the 15- by 20-in. subsonic wind tunnel, which has a vented test section with Plexiglass walls. The model was pressure-tapped at center span. Lift and pitching moment coefficients were obtained by numerical integration of pressure tap readings as recorded on a multiple-port scanivalve readout system. These coefficients were corrected by the addition of jet reaction components. Standard solid blockage corrections[3] were applied to the measured free-stream dynamic pressure; no wake blockage factor was used because of the uncertain effects of the jet.

Drag measurements were made by using a wake rake placed approximately 1.5 chord lengths downstream of the model inclined at 15 deg to the free stream. The rake employs 54 total and 8 static tubes, with the heaviest concentration of tubes near the center height. The momentum deficit methods of Betz and Jones[4] were then used to determine the drag coefficient. To account for the increase in momentum from the Coanda jet, an addition of $\dot{m}\, V_\infty/q_\infty S$ was made to the drag coefficient.

Wall blowing was employed to ensure that test conditions were as close as possible to two-dimensional flow (especially at high-lift conditions). Two sets of plenums were embedded in each of the tunnel walls, one ahead of the leading edge and the other at approximately the 70-percent chord position. The blowing rates of the two sets of wall jets were adjusted independently and in accordance with the model blowing rate. The wall jets were used to energize the wall boundary layer to prevent separation and to reduce the vorticity associated with induced effects. Spanwise pressure taps were employed to record the lateral pressure distribution as an indication of the two-dimensionality.

Mass flow rate $\dot{m}$ was measured by a calibrated orifice plate inserted in the supply line. The jet velocity was calculated by assuming isentropic expansion from duct stagnation pressure to the free-stream static pressure as follows:

$$V_j = a_j M_j = (\gamma R T_j)^{1/2} M_j = \left\{ 2RT_t \left(\frac{\gamma-1}{\gamma}\right) \left[1-\left(\frac{P_\infty}{P_t}\right)^{(\gamma-1)/\gamma} \right] \right\}^{1/2}$$

The momentum coefficient was then defined as $C_\mu = (\dot{m} V_j / q_\infty S)$.

A series of runs were made at free-stream dynamic pressures from 10 to 50 lb/ft^2 (478.8 to 2394.0 N/m^2) corresponding to a model Reynolds number range of 0.38×10^6 to 0.845×10^6 (Figure 2). In general, no significant effect on the data over this Reynolds number range was noted, and due to limitations on the internal duct pressure, q_∞ = 20 lb/ft^2 (957.6 N/m^2) was chosen to allow for a wider range of C_μ.

RESULTS AND DISCUSSION

Airfoil characteristics were evaluated for three slot height-to-chord ratios of 0.0010, 0.0015, and 0.00225 (h = 0.008, 0.012, and 0.018 in.; 0.203, 0.305, and 0.457 mm) for angles of attack α ranging from -20 to 6 deg and momentum coefficients C_μ ranging from 0 to 0.24. Figure 3 depicts the variation of momentum coefficient with duct pressure for the three slot height-to-chord ratios for a dynamic pressure of 20 psf (957.6 N/m^2).

The expansion of the slot caused by pressurization of the duct at h/c = 0.0015 is shown in Figure 4. These data were obtained by pressurizing the duct and measuring the resulting slot height with a thickness gage under quiescent tunnel conditions.

LIFT

Figures 5a and 5b show the sectional lift coefficient as a function of momentum coefficient for h/c = 0.0015, 0.0010, and 0.00225. The data are also presented in Figure 5c on an expanded scale as a function of momentum coefficient for h/c = 0.0015. An examination of this figure reveals a discontinuity in the lift curve slope at α = -2, -4, and -8 deg, which is similar to that found with a previous model. Because this discontinuity had previously been associated with a region of separated flow occurring ahead of the slot at very low values of the momentum coefficient, it was hypothesized that this effect might be prevented by placing a trip strip on

the model upper surface. Figure 5d shows that the placing of a trip strip at the three chordal positions resulted in a continuous curve, thus indicating a probable dependence on Reynolds number.

Figure 5a shows that with the exception of α = 6 deg, lift coefficient continually increases with increasing momentum coefficient, indicating that "C_μ stall" has not as yet been reached; therefore, it appears that the lift coefficient could have been increased still further with increased blowing. At α = 6 deg a decrease in the lift coefficient is observed for $C_\mu > 0.143$. This loss in lift corresponds to a loss in the leading edge suction peak, as observed on the plot of pressure coefficients on the airfoil; see Figure 6a. A maximum lift coefficient of 4.53 was reached at α = 2 deg and C_μ = 0.22.

Examination of the plots of pressure coefficient at α = -20 deg indicates that initially flow separation occurs on the entire lower surface; however, positive values of lift coefficient are still generated. As blowing increases, the leading edge stagnation point which is on the upper surface moves forward due to the increasing circulation, resulting in flow attachment at $C_\mu \simeq 0.1$. Further examination of the plots of pressure coefficient (Figure 6b) indicates that at h/c = 0.0015, for all alphas except -20, -12, and -8 deg, there appears at some point in the test range a large change in pressure coefficient between the same two leading edge pressure taps. The same pattern persists at α = 0 deg for h/c = 0.0010 and 0.00225 and was previously noted with another circulation control model. Potential flow plots of several of the experimental conditions indicate that this phenomenon is probably a result of the leading edge geometry.

A comparison of the lift characteristics for h/c = 0.001 and 0.0015 (Figure 5a and 5b) indicates that an increase in lift coefficient for a given value of momentum coefficient is achieved at the smaller slot height-to-chord ratio, especially at the moderate and higher blowing rates. At h/c = 0.0010, a $C_{\ell_{max}}$ = 4.44 was obtained at C_μ = 0.175 (due to constraints on internal duct pressure this is the maximum attainable momentum coefficient). This is in contrast to C_ℓ = 4.05 for a compariable value of momentum coefficient at h/c = 0.0015. A typical pressure distribution for

both slot heights is presented in Figure 6c. A comparison of the results for h/c = 0.0015 and 0.00225 indicates, in general, that for a given momentum coefficient a decrease in lift coefficient is noted. This decrease may be due in part because an increase in slot height for a given momentum coefficient will correspond to a decrease in jet velocity at the slot exit and therefore a decrease in the kinetic energy of the Coanda jet. This reduction in the kinetic energy may effect the turning capability of the jet.

Figure 7a depicts the augmentation ratio as a function of momentum coefficient for h/c = 0.0015. The augmentation ratio is defined as $\Delta C_\ell / C_\mu$, where ΔC_ℓ is the increase in lift coefficient above the unblown value for a given momentum coefficient and incidence. Since the maximum augmentation coincides with the discontinuity in the lift curve slope in Figure 5c, the augmentation ratio achieved with trip strips placed on the model is of more practical interest. Figure 7b presents these data at α = 2 deg for the various trip strip locations. An augmentation ratio in excess of 80 is achieved at C_ℓ = 0.36 with the trip strip at x/c = 0.4. In comparing Figures 5d and 7b, note the sensitivity of maximum augmentation to the precise slope of the lift curve at the very low values of momentum coefficient. In Figure 7a, a significant loss in augmentation is apparent at α = -20 deg, to a lesser extent at α = 6 and 2 deg, and the remaining data fall within a narrow band. In comparing the results in Figures 7a and 7c for the various slot heights, the highest maximum augmentation occurs at h/c = 0.0010, while a considerable loss is noted at h/c = 0.00225.

Because the model was designed to operate at transonic speeds, emphasis was placed on providing a high critical Mach number without unduly compromising subsonic performance. To ascertain how well the proposed airfoil would accomplish this, a finite difference technique developed by Rogers[6] was employed during the design phase. This procedure involved the solution of the full inviscid compressible flow equations. Good agreement between the subsonic experimental data and potential flow had previously been established for circulation control airfoils, and thus the inviscid nature of the solution was not considered to be crucial. The analytically

predicted M_{crit} is shown in Figure 8 with the M_{crit} obtained by applying the Karman-Tsien compressibility correction to the subsonic experimental value of $C_{p_{min}}$ as a function of lift coefficient. Good agreement between the finite difference and extended subsonic data is noted for most cases; however, the exception is $\alpha = -4$ deg at $C_\ell = 0.65$ where the predicted M_{crit} is higher than that indicated by the extended subsonic data. For both the experimental and analytical data, the minimum pressure coefficient occurs on the upper surface in the vicinity of the slot and may result in the following difficulties. First, no modeling of the Coanda jet is made in the inviscid analysis. Thus, the trailing edge suction peak may be underestimated. The second difficulty is a limitation of the compressibility factor technique. As detailed by Rogers,[6] correction techniques including Karman-Tsien do not fully account for the effects of compressibility, particularly in a region of high acceleration. This would lead to discrepencies between the actual and predicted values of the trailing edge suction peak resulting in inaccurate estimates of M_{crit} based on subsonic data. Fortunately, the conditions under which the above difficulties arise usually occur outside of the area of prime interest.

Figure 8 indicates that both the experimental and analytical data predict a maximum M_{crit} in excess of 0.7 at $\alpha = -2.0$ deg for $-0.2 \leq C_\ell \leq 0.35$. The experimental values of the minimum pressure coefficient $C_{p_{min}}$ produced on the airfoil, and upon which the compressibility factor technique is based, is presented in Figure 9 for a given lift coefficient.

The variation of lift coefficient with geometric angle of attack is shown in Figure 10. The slope of the curves is similar for nonstall conditions, thus indicating that the C_ℓ,α relationship is not influenced by the level of blowing.

DRAG

The variation of a modified drag coefficient with momentum coefficient is presented in Figures 11a and 11b for h/c = 0.0015, 0.0010, and 0.00225.

Figure 11c presents data at low values of momentum coefficient on an expanded scale for h/c = 0.0015. These data result from an integration of the wake deficit using the method of Betz[4] which was then modified to account for the additional momentum of the jet, thereby becoming $C_d = C_{d_{rake}} - (\dot{m}V_\infty/qS)$. The initial unblown drag levels are high due to the nature of bluff trailing edge airfoils; however, with the onset of blowing, a reduction in drag is noted at most angles of attack. Negative drag levels, a product of effective thrust recovery, are achieved at relatively low values of blowing coefficient for all angles of incidence except α = -20 deg (see Figure 11a). The high level of drag that exists at α = -20 deg is attributed to the extensive flow separation which occurs on the lower surface of the model. The drag rise at α = +6 deg (h/c = 0.0015) coincides with the degradation in lift coefficient observed in Figure 5a. At α = -8 and -12 deg a hump in the drag curve is noted for which no satisfactory explanation can be made.

An examination of the results presented in Figure 11b for h/c = 0.00225 indicates a drag rise for $C_\mu > 0.142$ at all angles of incidence. This rise in the drag coefficient coincides with a change in the pressure distribution on the last 20 percent of the model lower surface, as shown in Figure 12.

PITCHING MOMENT

The pitching moment about the midchord ($C_{m_{50}}$) as a function of momentum coefficient is depicted in Figure 13. The high trailing edge suction peak produces the negative pitching moment, which has been typical of previous circulation control airfoils.

EQUIVALENT LIFT-TO-DRAG RATIO

An equivalent lift-to-drag ratio is defined which takes into account the energy expended to produce blowing and thus allows a direct comparison between the performance of a circulation control airfoil section and an

unblown airfoil. The equivalent drag is defined as:

$$d_e = d + \frac{P_{comp}}{V_\infty} + \dot{m}V_\infty$$

where d = momentum deficit as measured by the drag rake (corrected for jet efflux)

P_{comp}/V_∞ = compressor power (kinetic energy flux)

$\dot{m}V_\infty$ = intake momentum flux (ram penalty)

The compressor power required may be expressed as:

$$P_{comp} = \frac{\dot{m}}{2}\left(\frac{2\gamma}{\gamma-1}\right) RT_d\left[1-\left(\frac{P_{ram}}{P_t}\right)^{(\gamma-1)/\gamma}\right]$$

If intake losses are assumed to be negligible, then the ram pressure is equal to the free-stream total pressure. For subsonic flows with $M_\infty \leq 0.2$, $P_{t_\infty} \simeq P_\infty$. Thus, the above equation becomes:

$$P_{comp} = \frac{1}{2}\dot{m}V_j^2$$

Substituting for P_{comp}, the coefficient form is then:

$$\frac{\ell}{d_e} = C_\ell/C_d + C_\mu \frac{V_j}{2V_\infty} + C_\mu \frac{V_\infty}{V_j}$$

The equivalent lift-to-drag ratio as a function of lift coefficient is presented in Figures 14a and 14b for h/c = 0.0015, 0.0010, and 0.00225.

The maximum ℓ/d_e generated was approximately 40 at $C_\ell = 0.8$, despite the relatively high value of maximum lift coefficients. Maximum efficiency for this airfoil is generated at positive angles of incidence and low blowing. The maximum ℓ/d_e for negative angles of incidence also occurs at low values of momentum coefficient. These results emphasize the need to produce high values of lift coefficient at low values of momentum coefficient to maintain high efficiency due to the prominence of the kinetic energy term $(C_\mu V_j/2V_\infty)$.

When comparing the results in Figure 14b at h/c = 0.0010 and 0.0025, note that a higher efficiency is reached at h/c = 0.0025 than at h/c = 0.0010. This higher maximum efficiency is reached despite a higher lift coefficient being attained at h/c = 0.001 for a given value of momentum coefficient. This is due mainly to the increase in the compressor power, which is proportional to $(V_j/V_\infty)^3$, required to produce the higher V_j for a given value of C_μ at h/c = 0.0010.

CONCLUSIONS

1. A maximum lift coefficient of 4.63 was reached at α = 2 deg for C_μ = 0.22. A lift coefficient in excess of 2 was generated by the section at α = -20 deg.

2. A continuous lift curve slope (dC_ℓ/dC_μ) was achieved at low blowing rates through the use of trip strips on the model upper surface, indicating that dC_ℓ/dC_μ is Reynolds number dependent at low values of blowing coefficient.

3. Decreasing the slot height-to-chord ratio from 0.0015 to 0.0010 resulted in an increase in lift coefficient for the same C_μ, especially at the moderate and higher blowing rates for the two angles of incidence tested. A decrease in the sectional lift coefficient is noted when the slot height-to-chord ratio is increased from 0.0015 to 0.00225.

4. At C_ℓ = 0.8, a maximum equivalent lift-to-drag ratio in excess of 40 was generated at h/c = 0.0015. A lower maximum efficiency was attained at both h/c = 0.0010 and 0.00225. Maximum efficiency is generated at

positive angles of incidence and at low values of momentum coefficient.

5. Augmentation ratios in excess of 65 were produced at α = -2, -4, and -8 deg at low blowing rates. With a trip strip placed at x/c = 0.4, augmentation ratios in excess of 80 were produced at α = -2 deg.

6. Both an analytical technique involving the solution of the full inviscid compressible flow equations and the Karman-Tsien compressibility correction applied to the experimental data were used to predict M_{crit}, with good agreement between both methods noted for most cases. The airfoil is predicted to have a maximum critical Mach number of 0.7 at typical operating conditions combined with a subsonic $C_{\ell_{max}}$ in excess of 4.5.

REFERENCES

1. Wilkerson, J.B., "An Assessment of Circulation Control Airfoil Development," DTNSRDC Report 77-0084 (Aug 1977).

2. Abramson, J., "Two-Dimensional Subsonic Wind Tunnel Evaluation of Two Related Cambered 15-Percent Thick Circulation Control Airfoils," DTNSRDC ASED Report 373 (Sep 1977).

3. Pope, A., "Wind-Tunnel Testing," Second Edition, John Wiley & Sons, Inc., New York (1964), pp. 307-311.

4. Schlichting, H., "Boundary Layer Theory," Sixth Edition, McGraw-Hill Book Company, New York (1968), pp. 708-713.

5. Abramson, J., "Two-Dimensional Subsonic Wind Tunnel Evaluation of A 20-Percent-Thick Circulation Control Airfoil," DTNSRDC Report ASED 331 (Jun 1975).

6. Rogers, E.O., "Numerical Solution of Subcritical Flow Past Airfoils," DTNSRDC Report 4112 (May 1973).

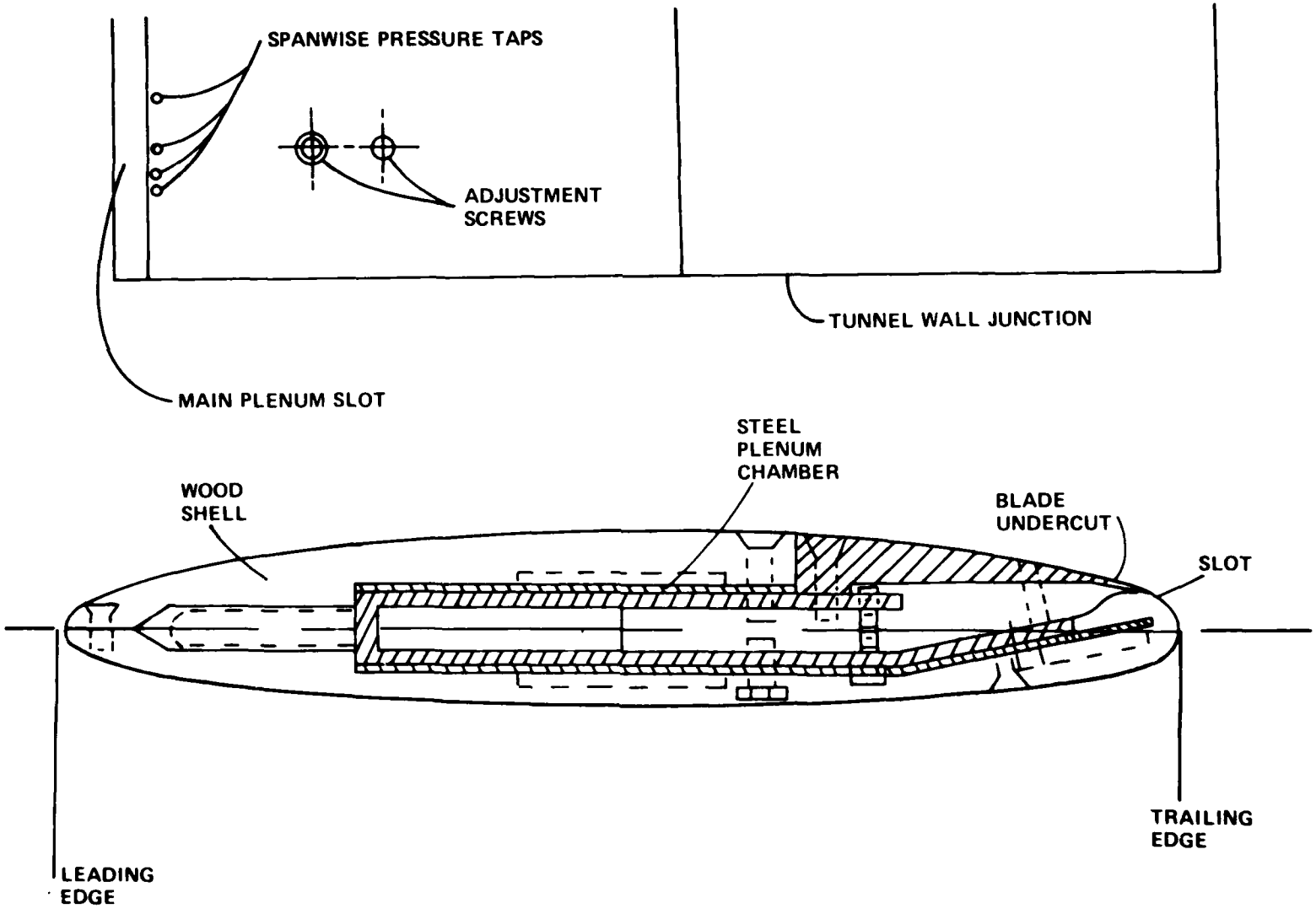

Figure 1 - Two-Dimensional Model Geometry

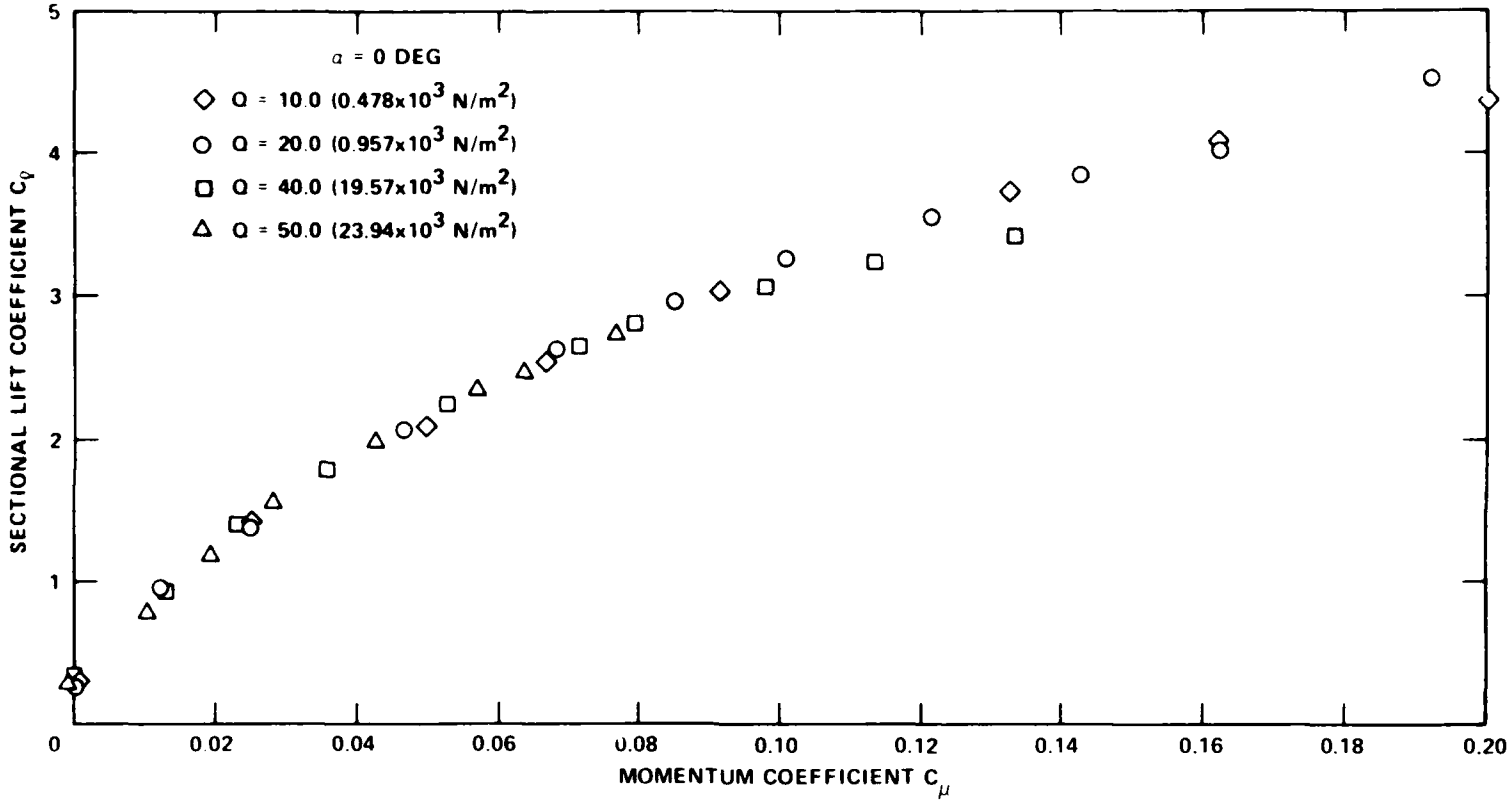

Figure 2 - Lift Variation with Dynamic Pressure

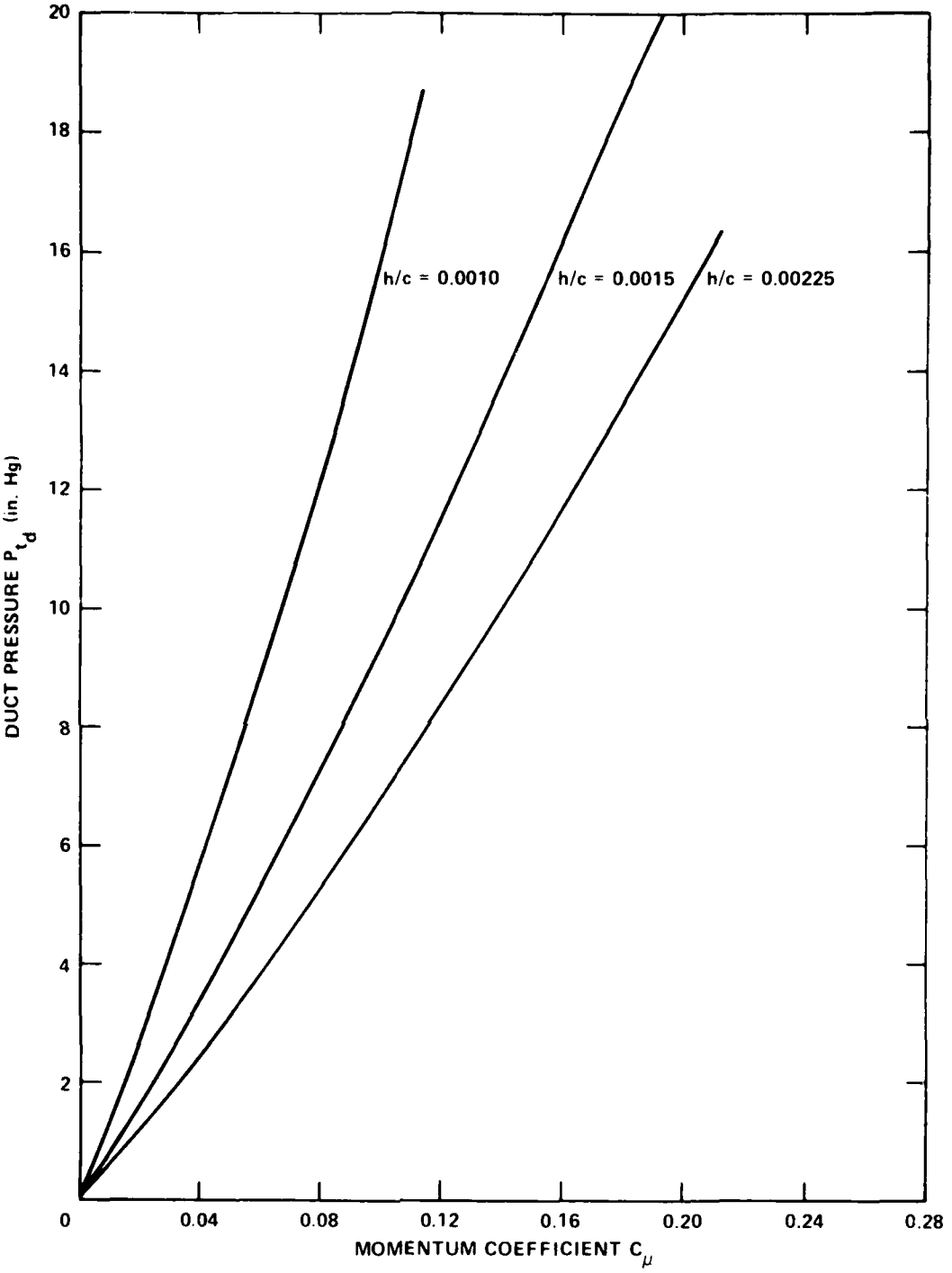

Figure 3 - Variation of Momentum Coefficient with Duct Pressure and Slot Height

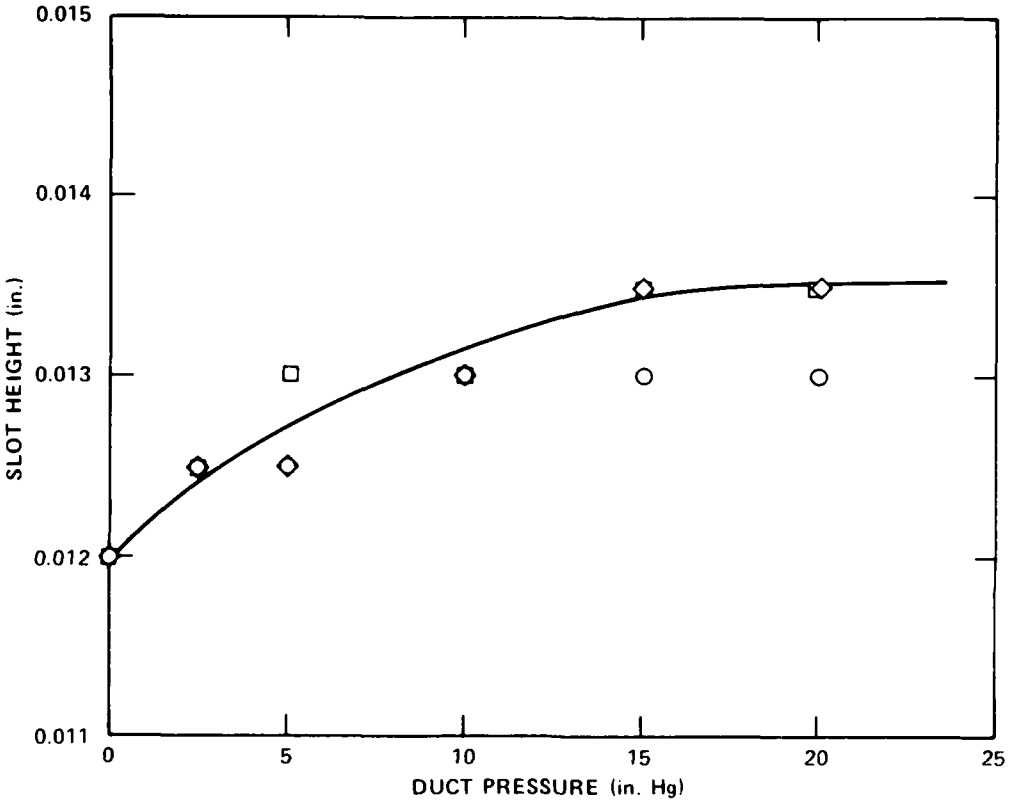

Figure 4 - Variation of Slot Height with Duct Pressure

Figure 5 - Lift Variation versus Momentum Coefficient

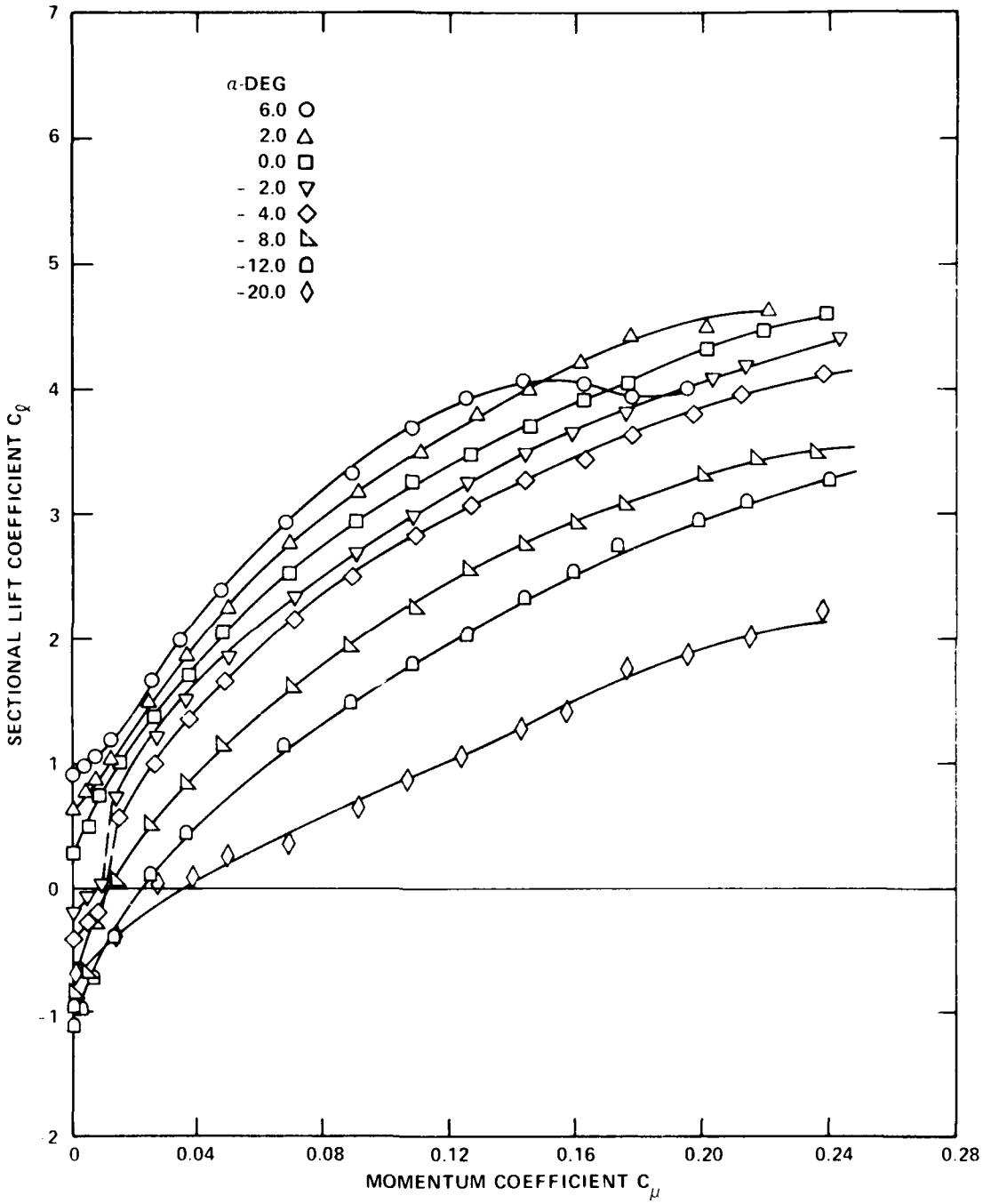

Figure 5a - h/c = 0.0015

Figure 5 (Continued)

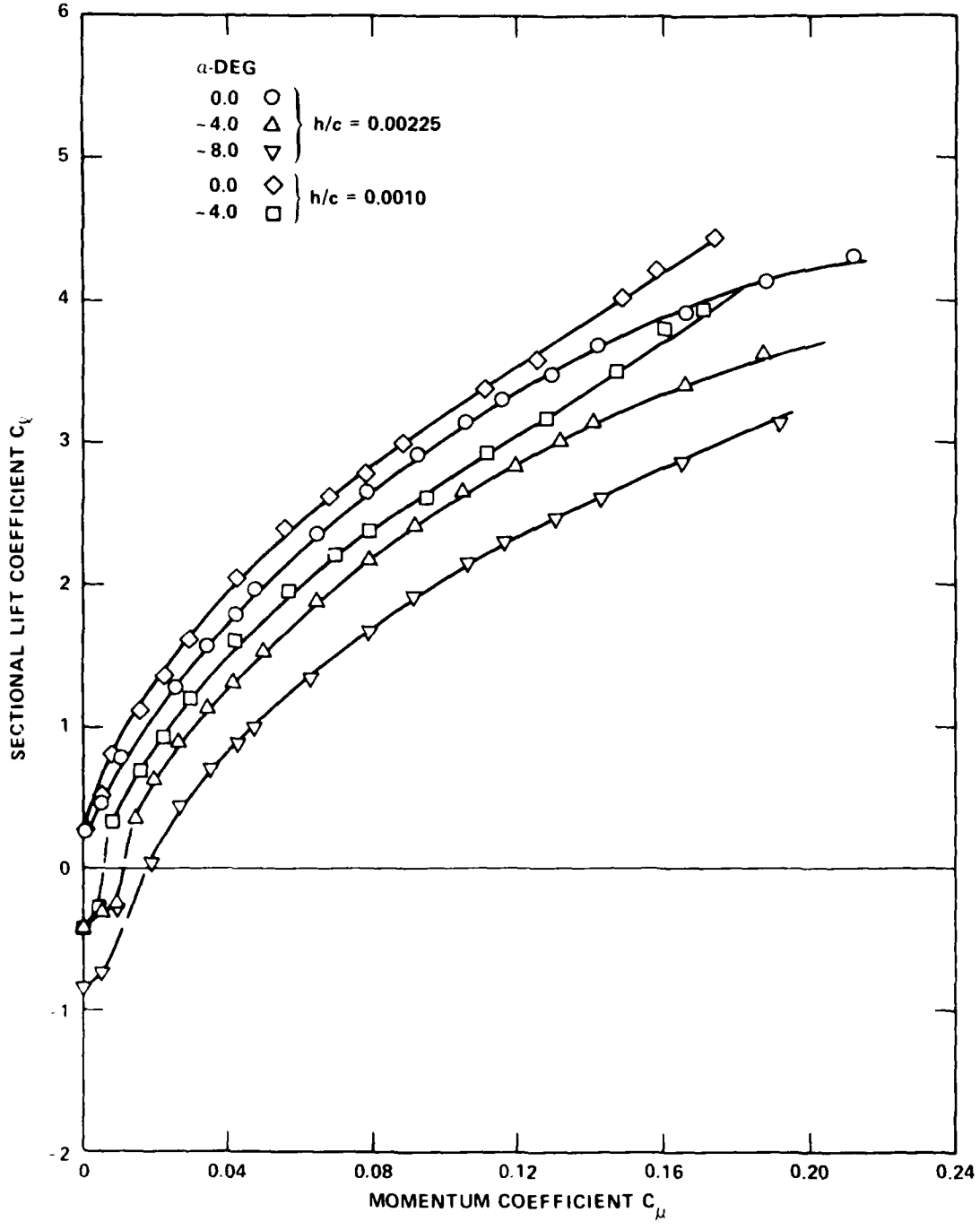

Figure 5b - h/c = 0.0010 and 0.00225

Figure 5 (Continued)

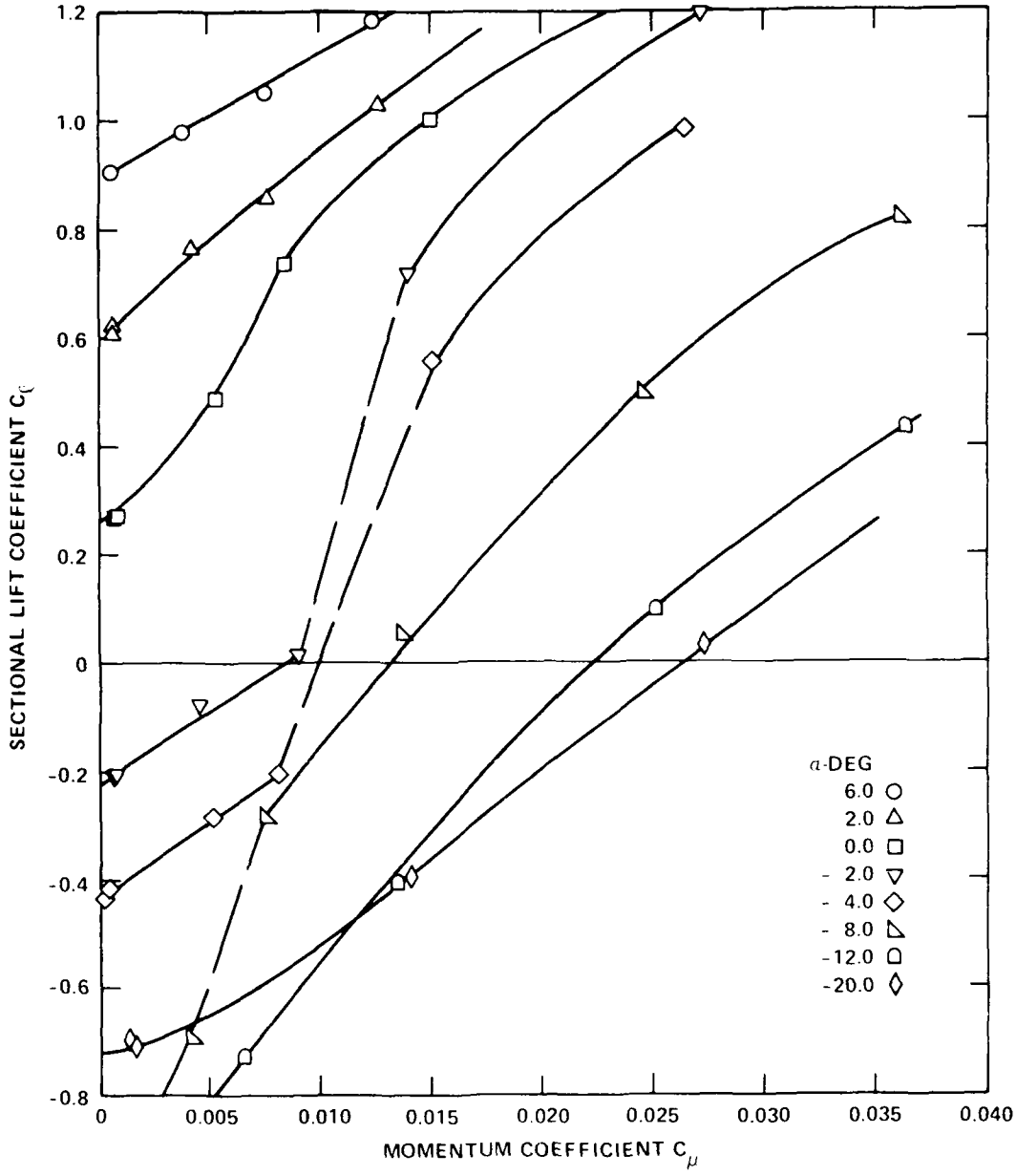

Figure 5c - h/c = 0.0015 (Expanded Scale)

Figure 5 (Continued)

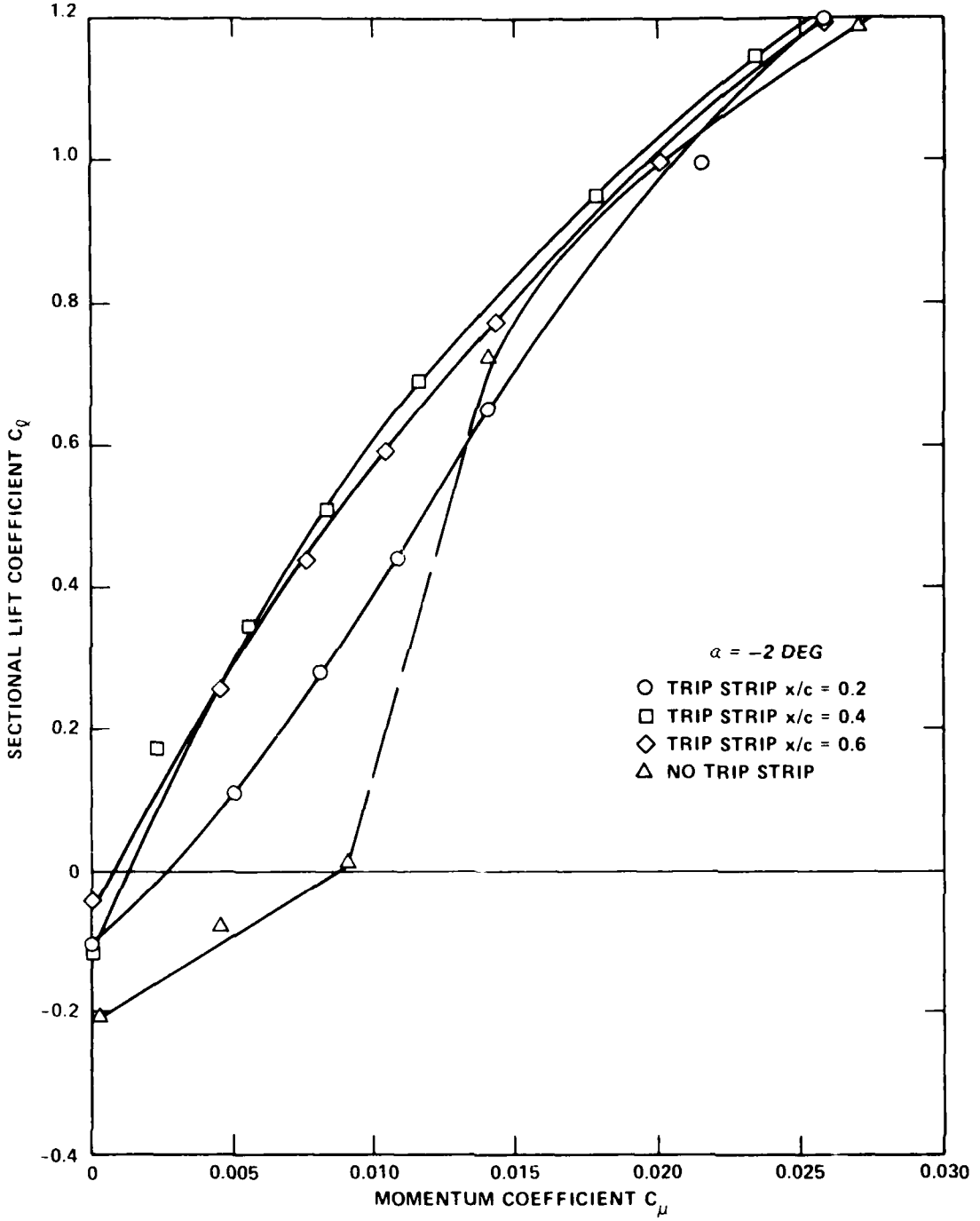

Figure 5d - With Trip Strip, h/c = 0.0015 (Expanded Scale)

Figure 6 - Experimental Pressure Distribution at Various Angles of Incidence

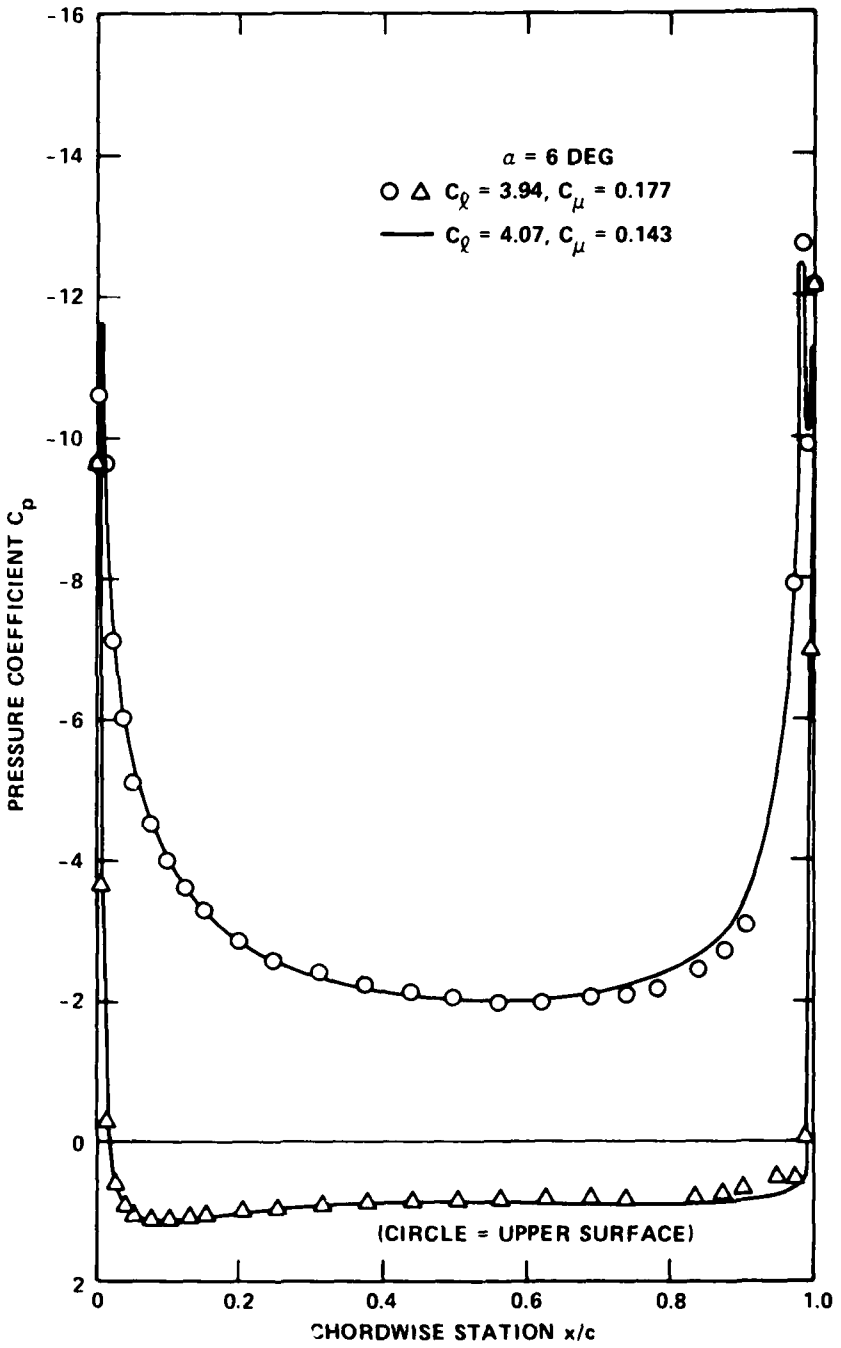

Figure 6a - α = 6 Degrees, h/c = 0.0015

Figure 6 (Continued)

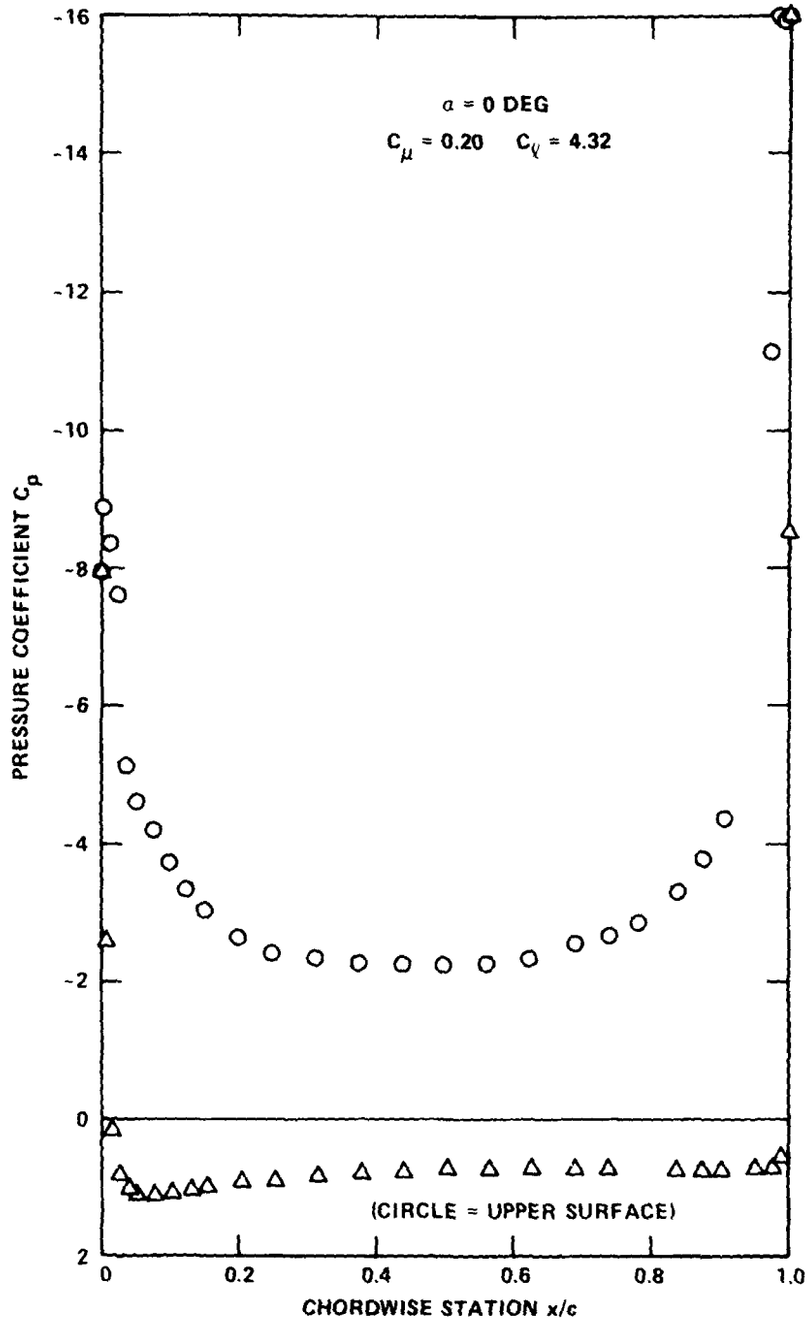

Figure 6b - α = 0 Degrees, h/c = 0.0015

Figure 6 (Continued)

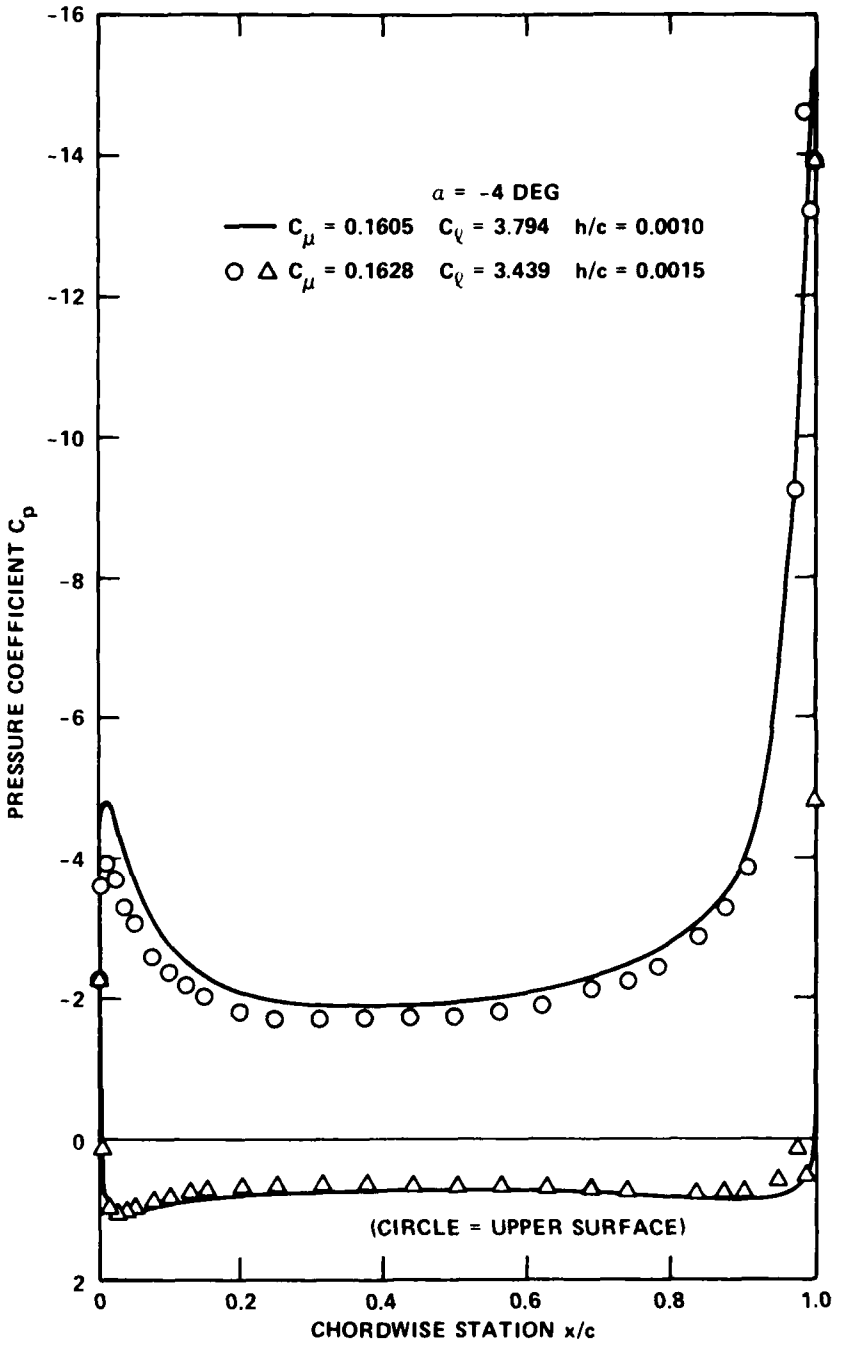

Figure 6c - α = -4 Degrees, h/c = 0.0010 and 0.0015

Figure 7 - Lift Augmentation Ratio versus Momentum Coefficient

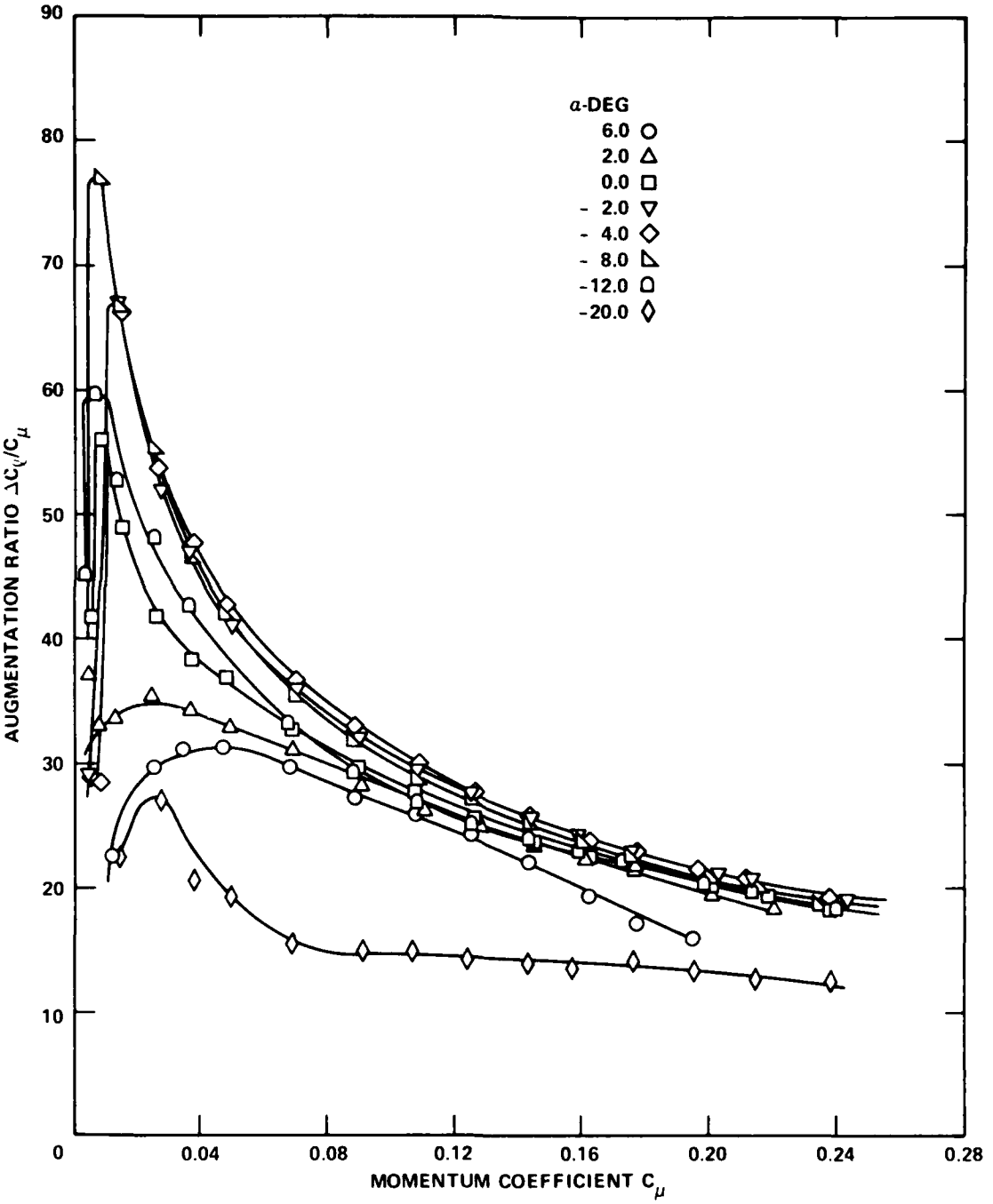

Figure 7a - h/c = 0.0015

Figure 7 (Continued)

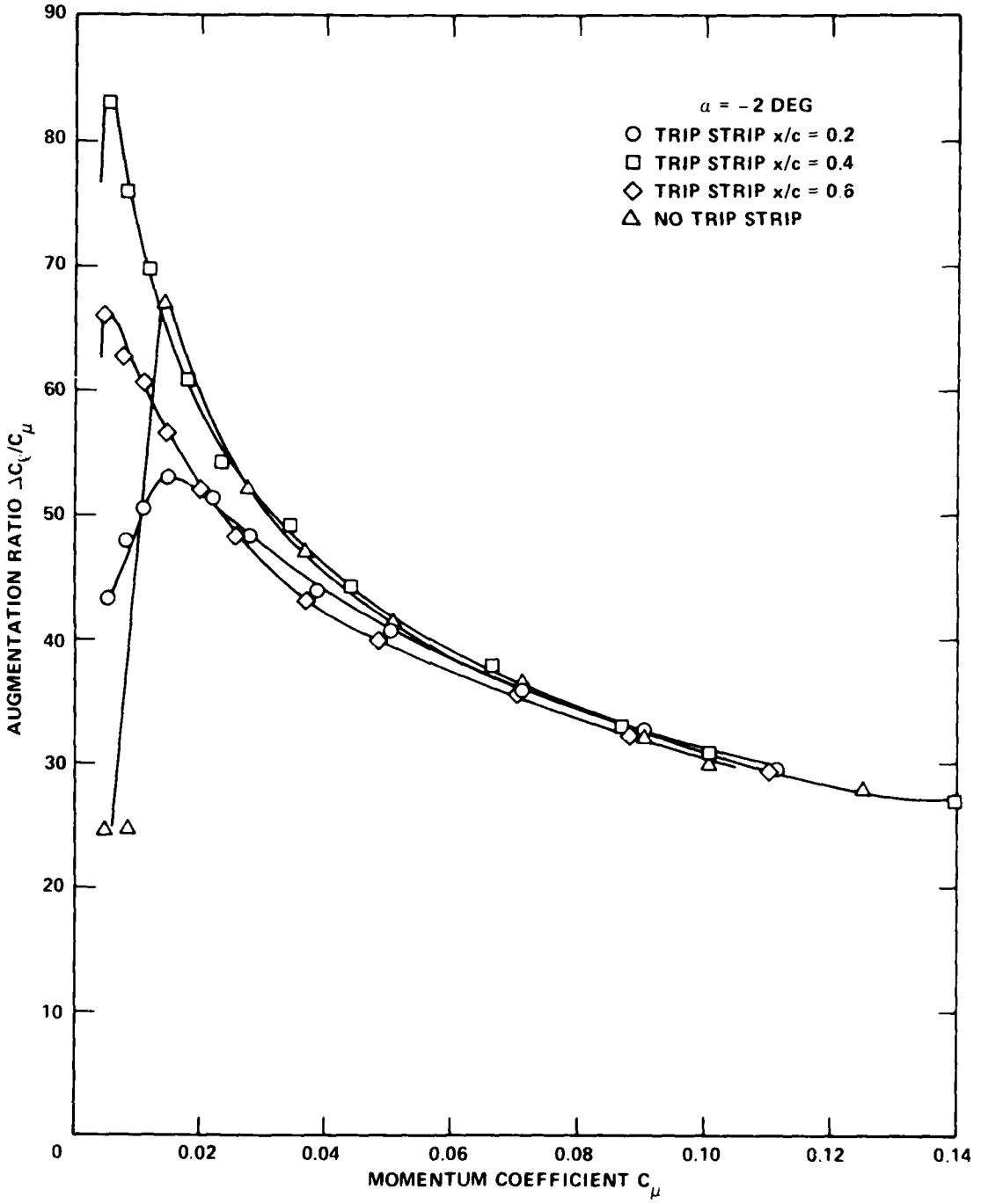

Figure 7b - With Trip Strip, h/c = 0.0015

Figure 7 (Continued)

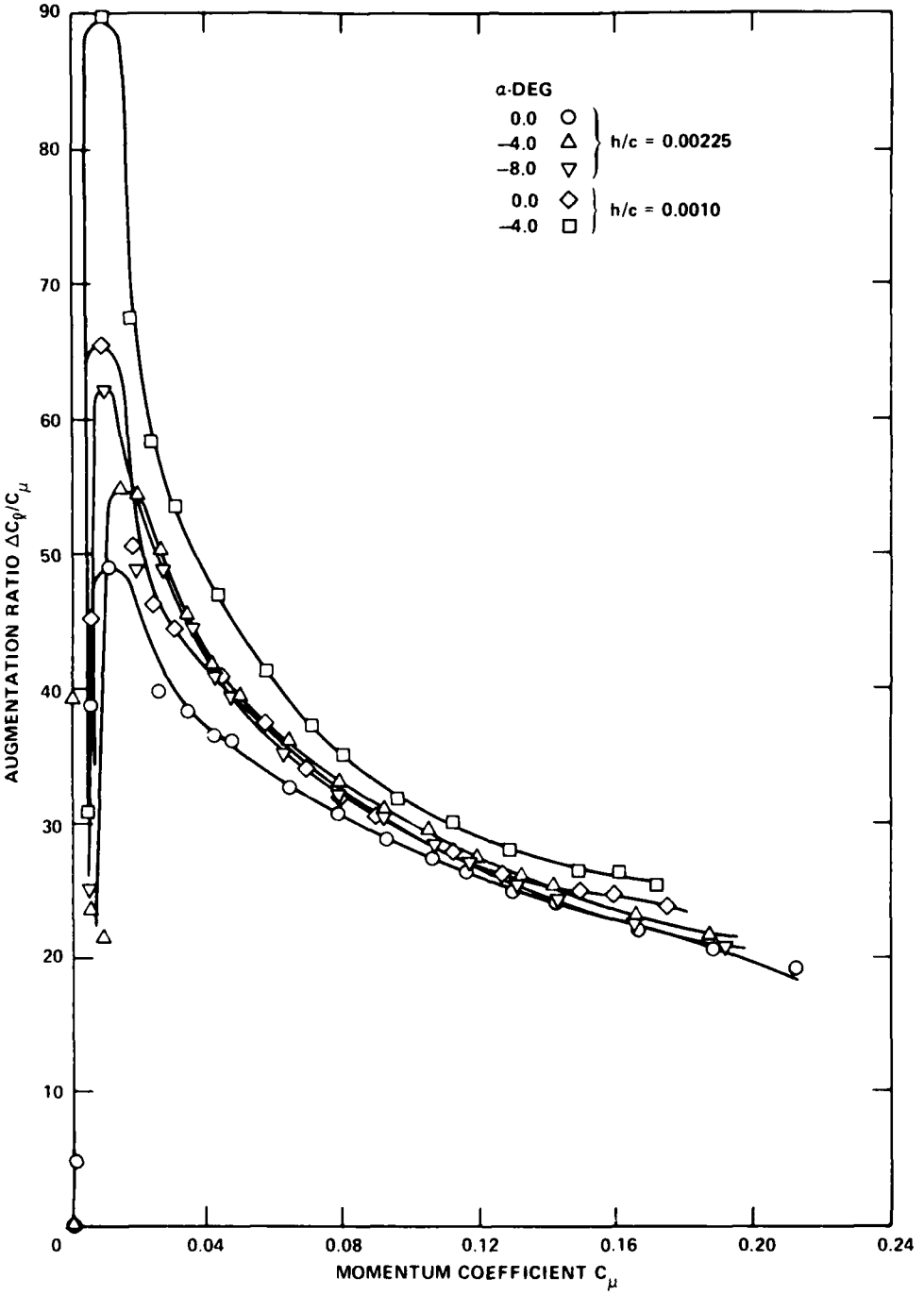

Figure 7c - h/c = 0.0010 and 0.00225

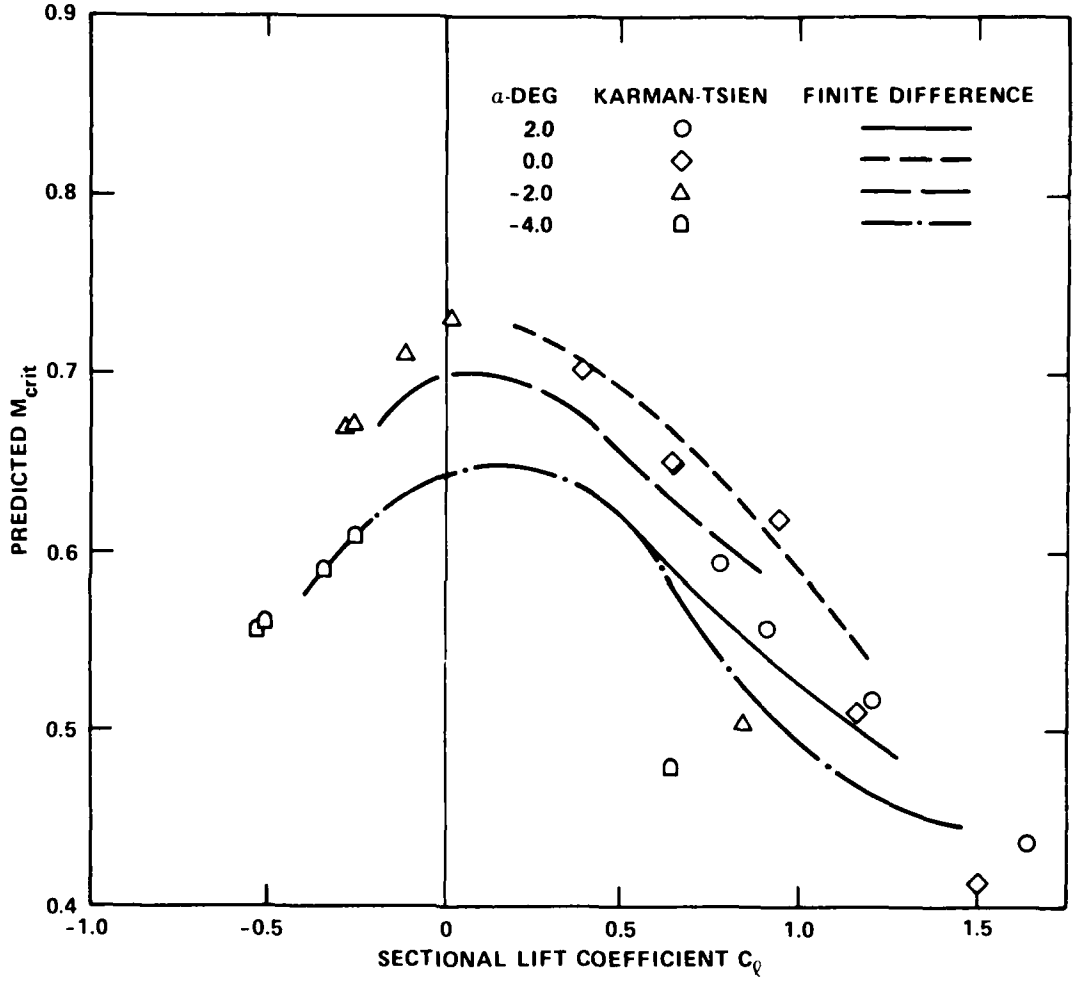

Figure 8 - Variation of Estimated M_{crit} with Lift Coefficient, h/c = 0.0015

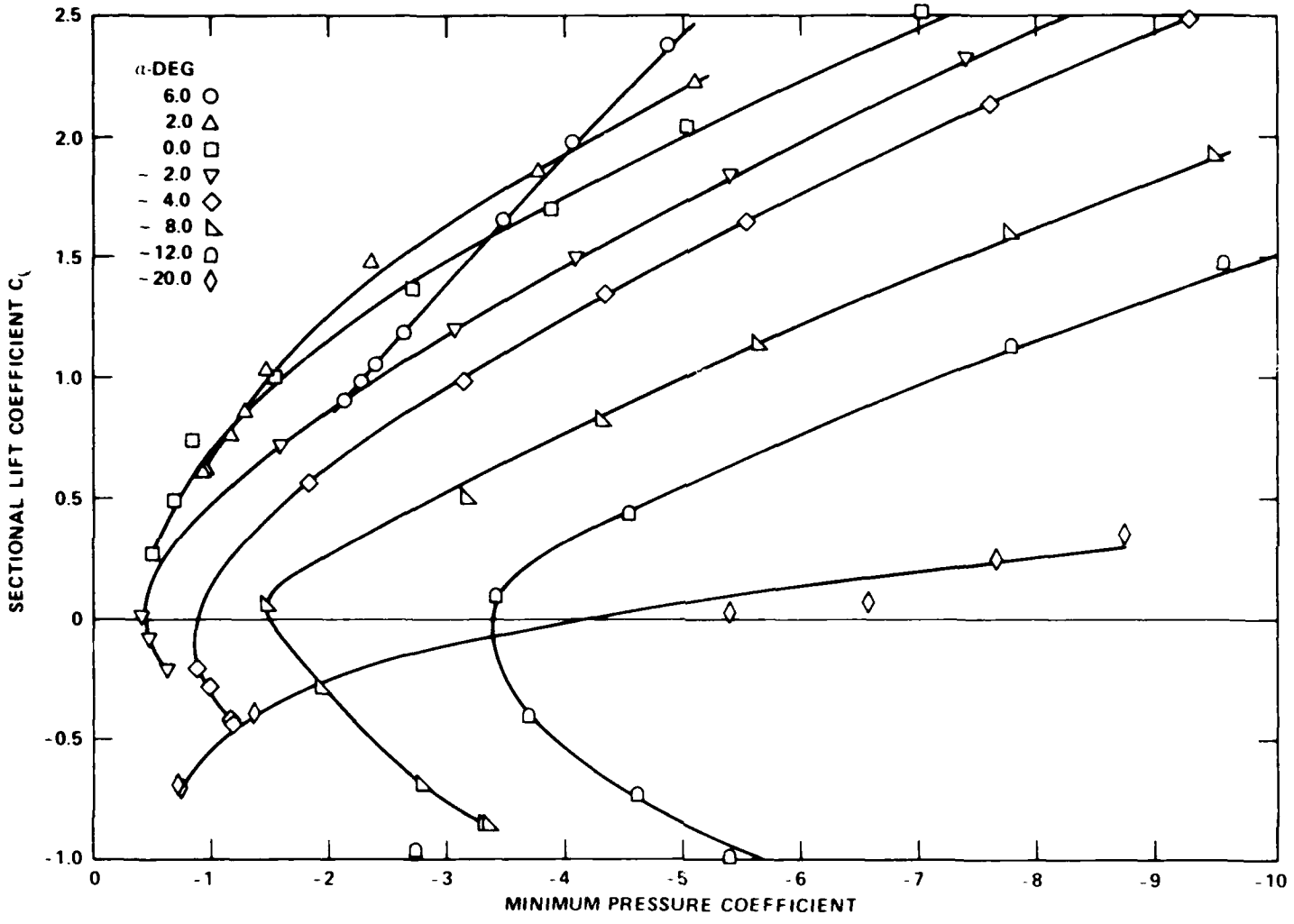

Figure 9 - Minimum Pressure Coefficient with Lift Variation, $h/c = 0.0015$

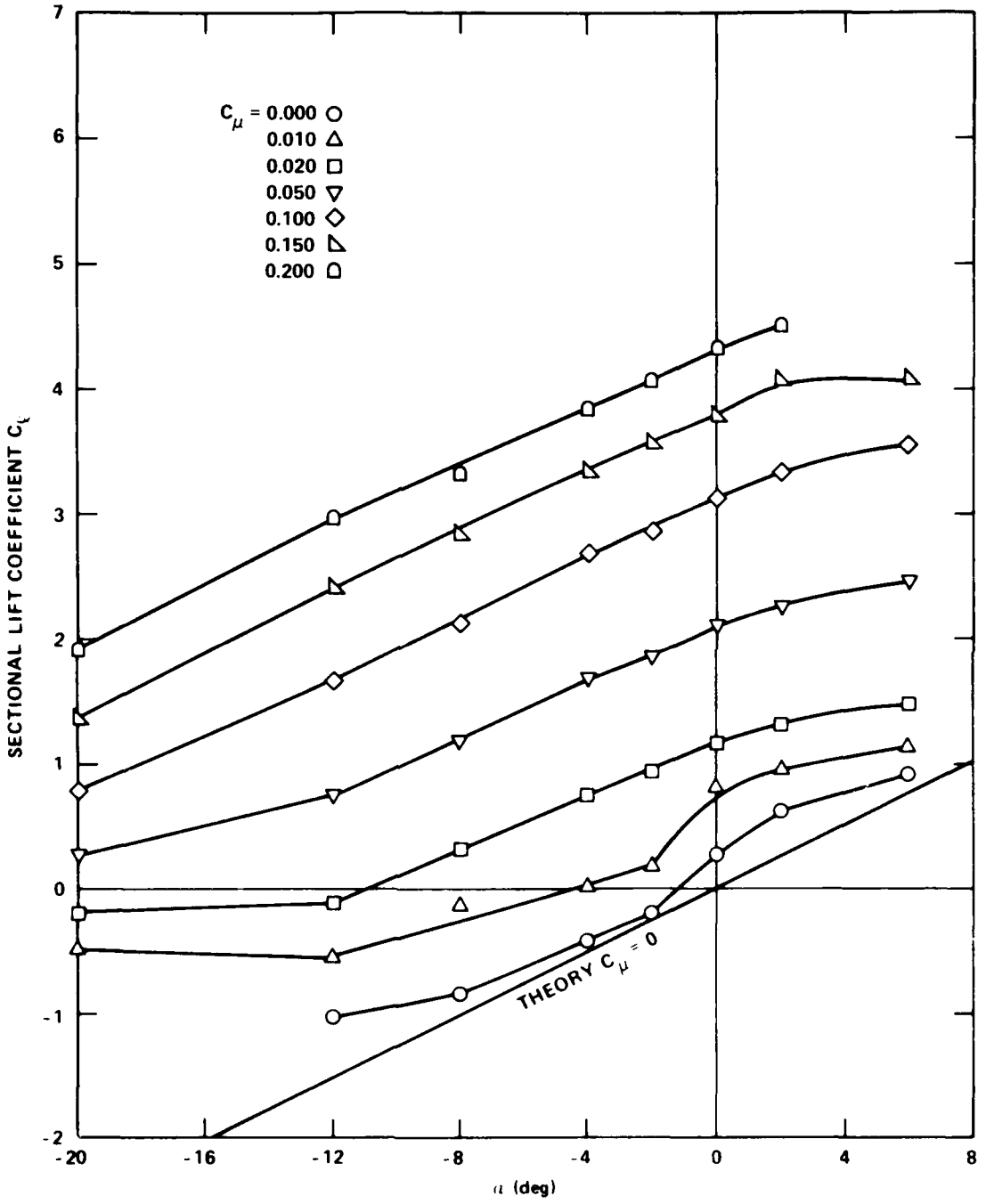

Figure 10 - Lift Variation with Geometric Angle of Attack, h/c = 0.0015

Figure 11 - Drag Coefficient versus Momentum Coefficient

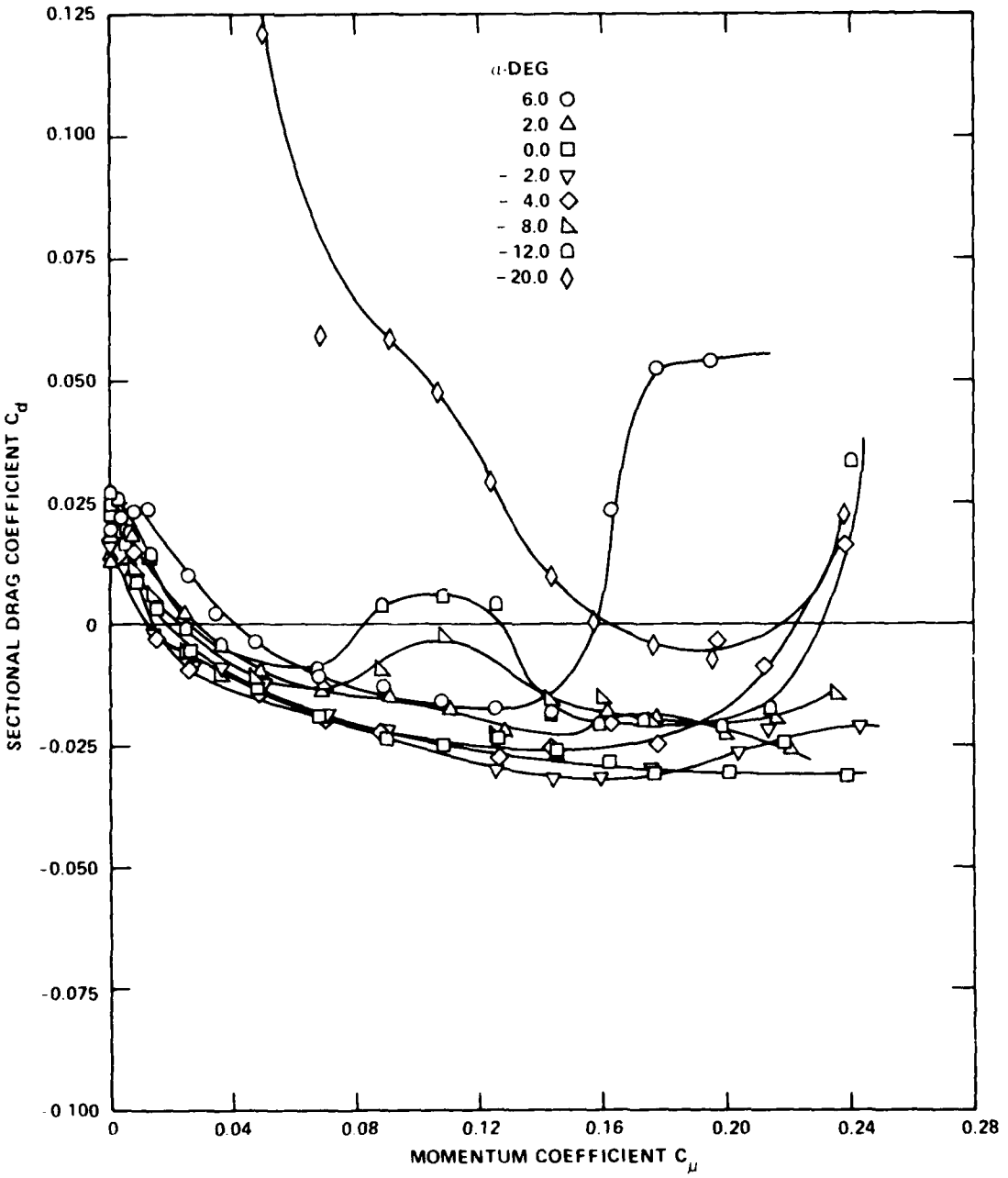

Figure 11a - h/c = 0.0015

Figure 11 (Continued)

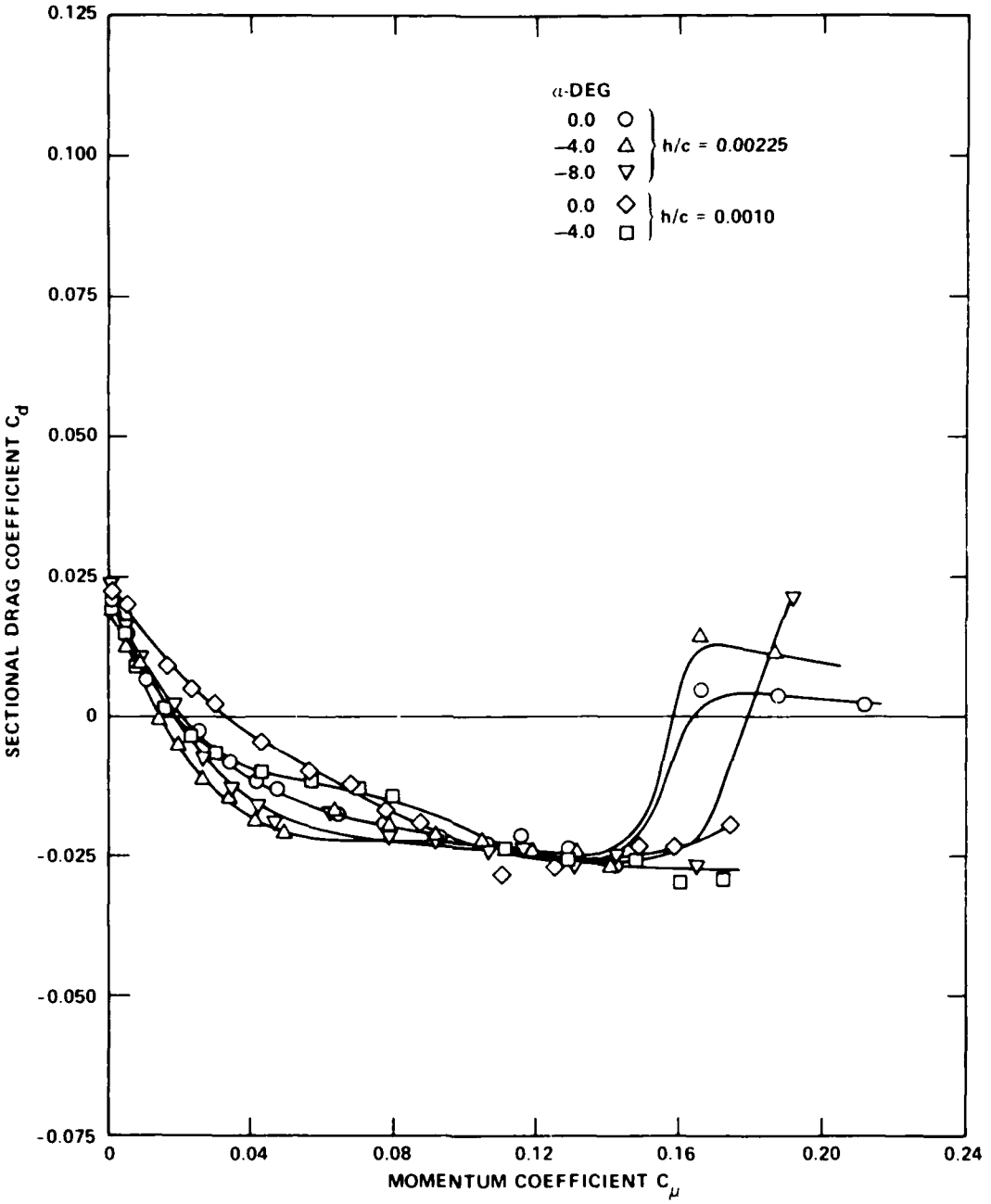

Figure 11b - h/c = 0.0010 and 0.00225

Figure 11 (Continued)

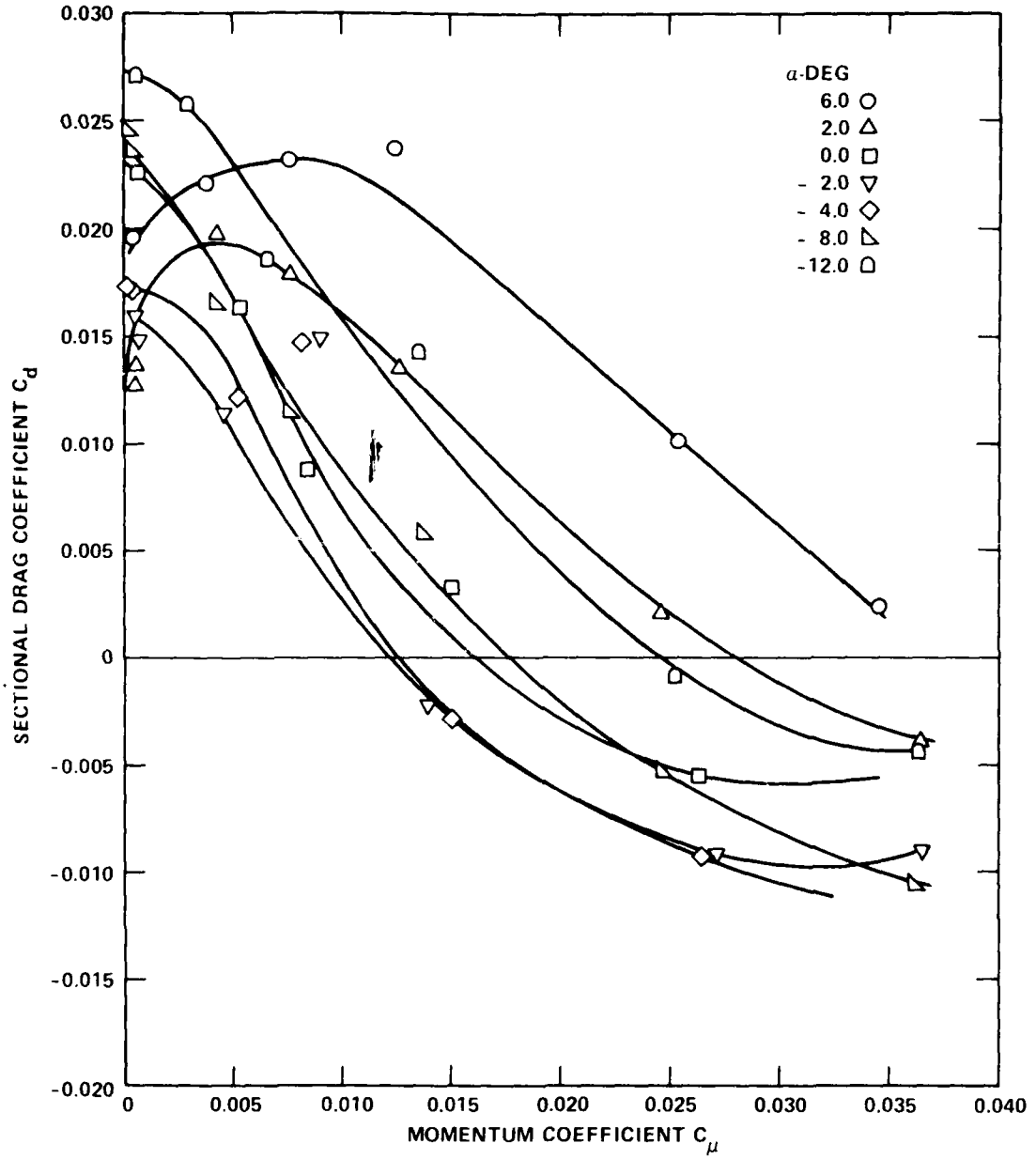

Figure 11c - h/c = 0.0015 (Expanded Scale)

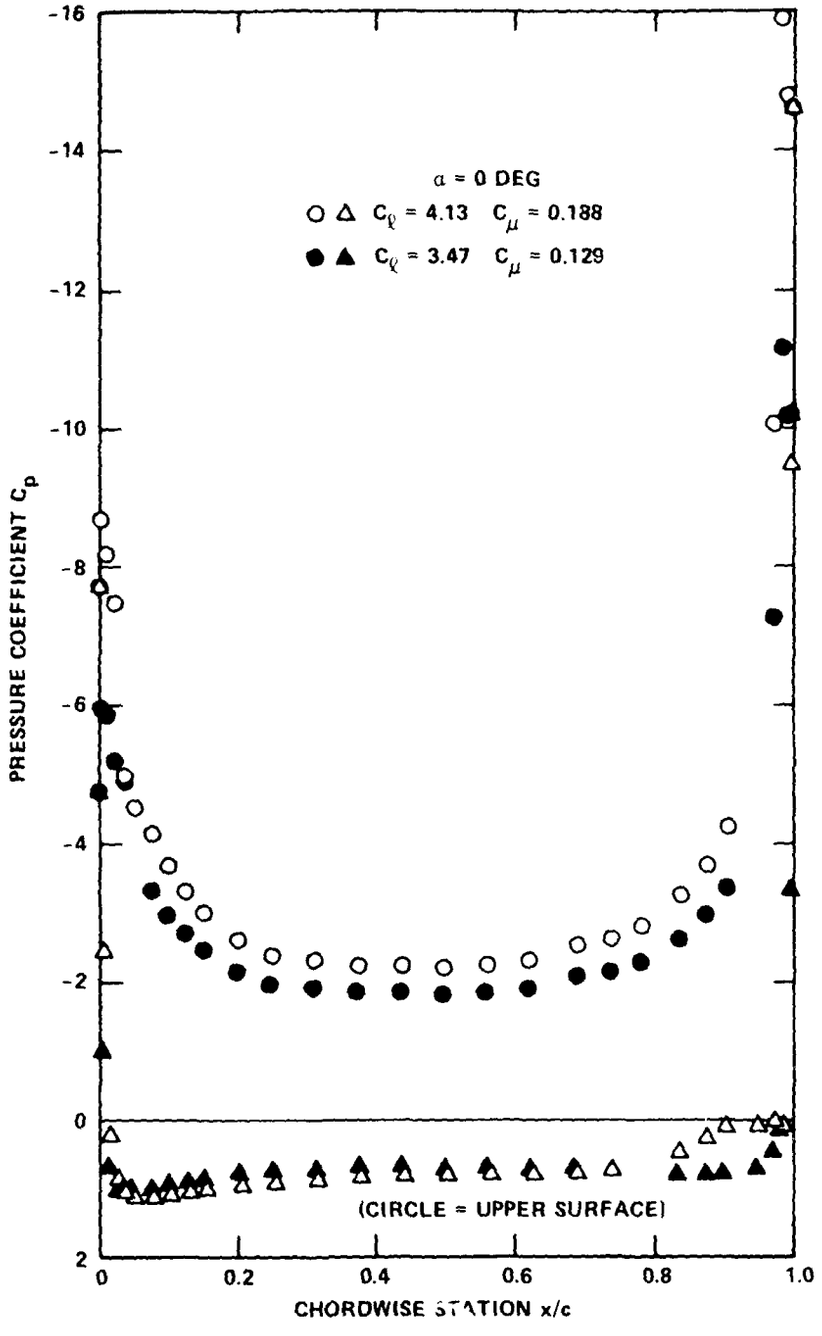

Figure 12 ~ Experimental Pressure Distributions
α = 0 Degrees, h/c = 0.00225

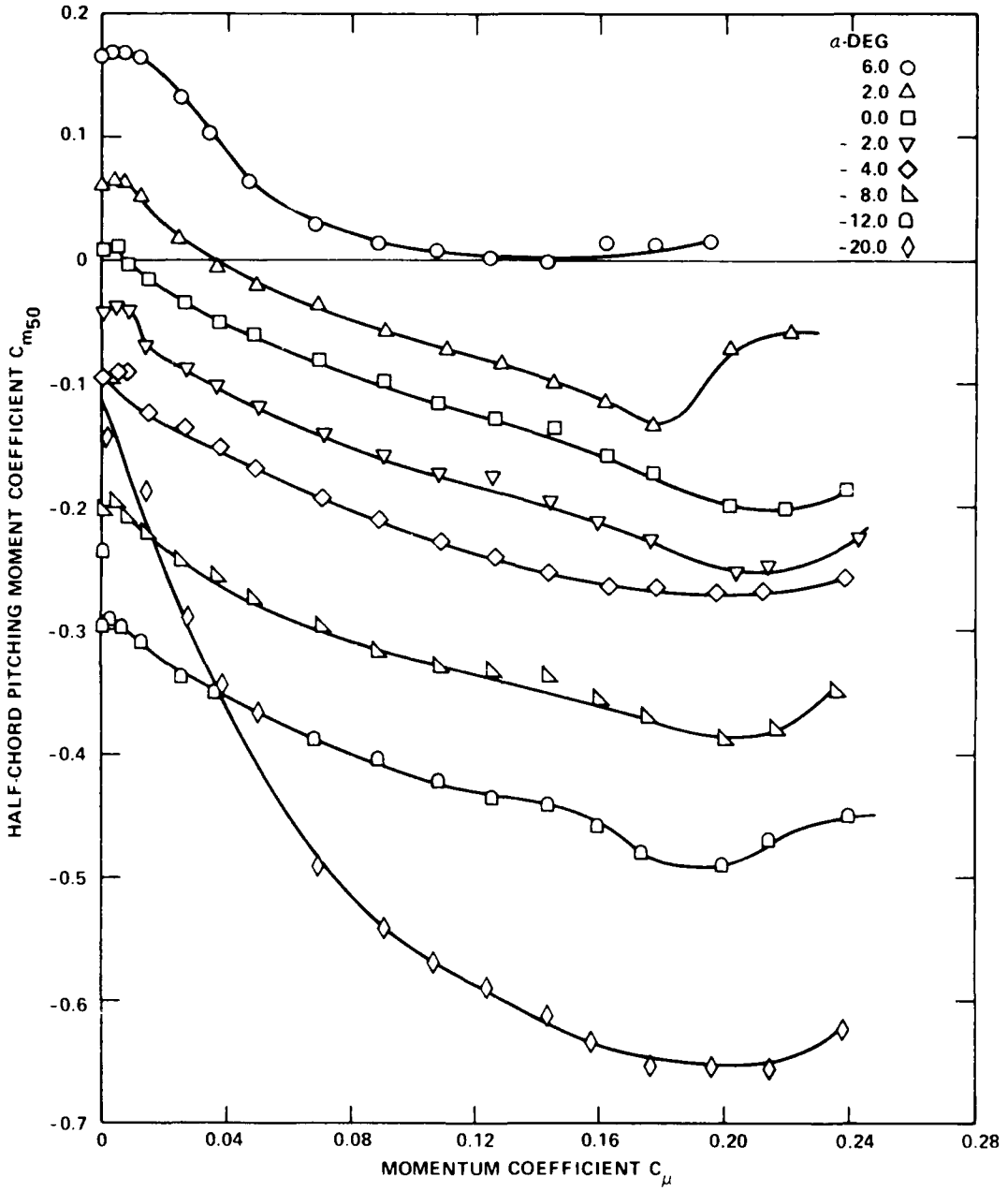

Figure 13 - Variation in Half-Chord Pitching Moment Coefficient versus Momentum Coefficient, h/c = 0.0015

Figure 14 - Equivalent Lift-to-Drag Ratio versus Lift Coefficient

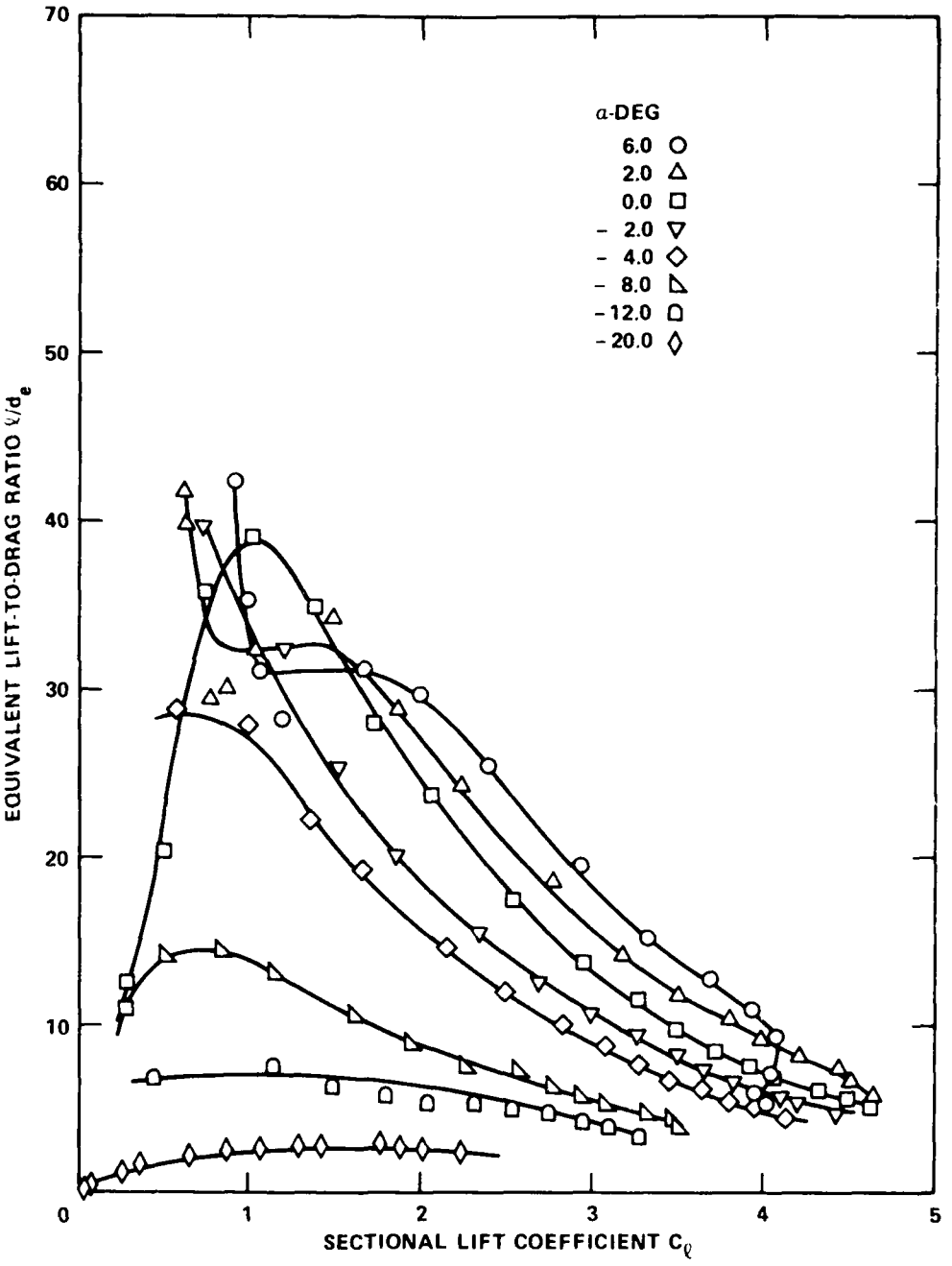

Figure 14a - h/c = 0.0015

Figure 14 (Continued)

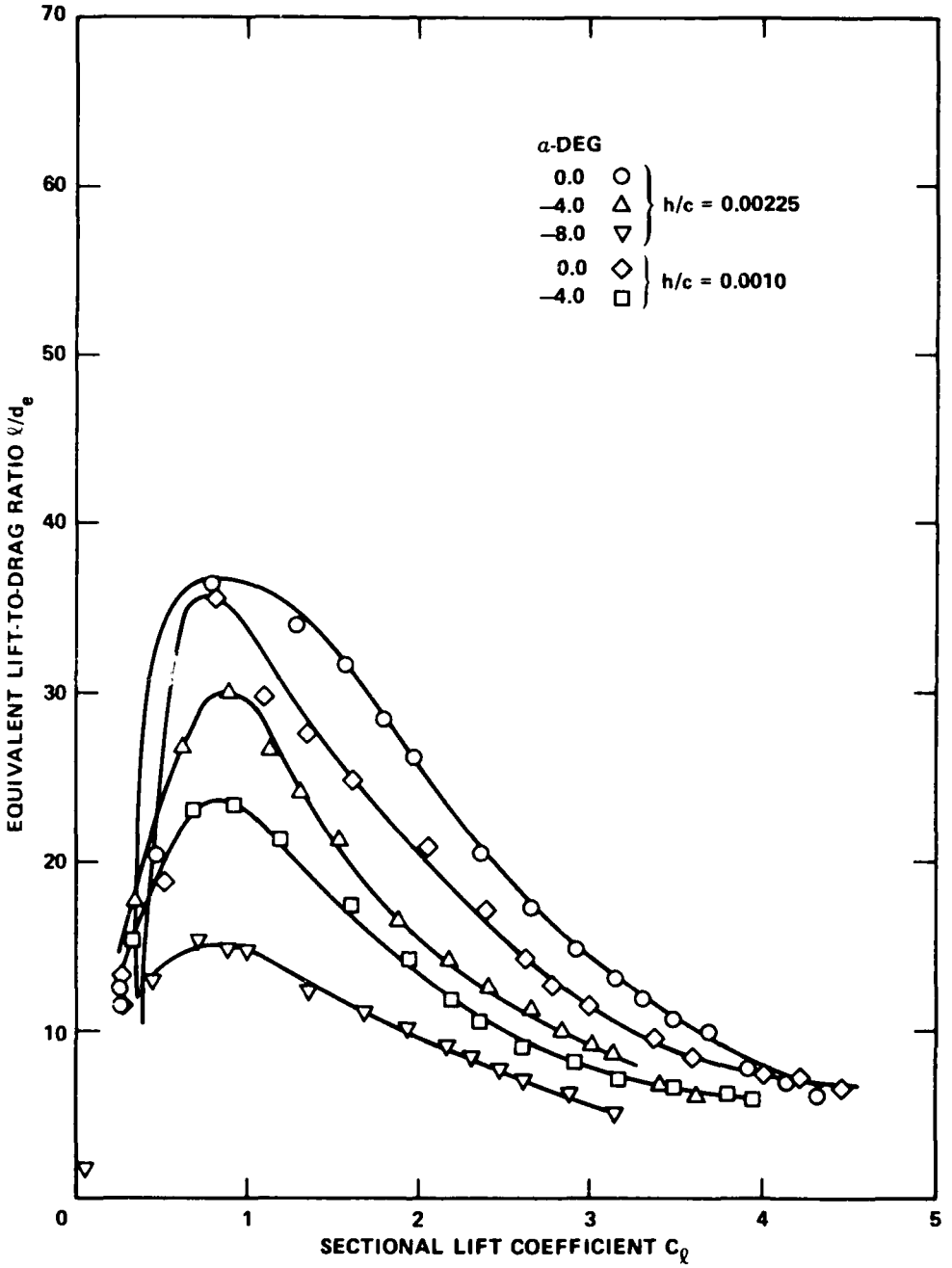

Figure 14b - h/c = 0.0010 and 0.00225

TABLE I – DESIGNATION FOR CIRCULATION CONTROL AIRFOILS

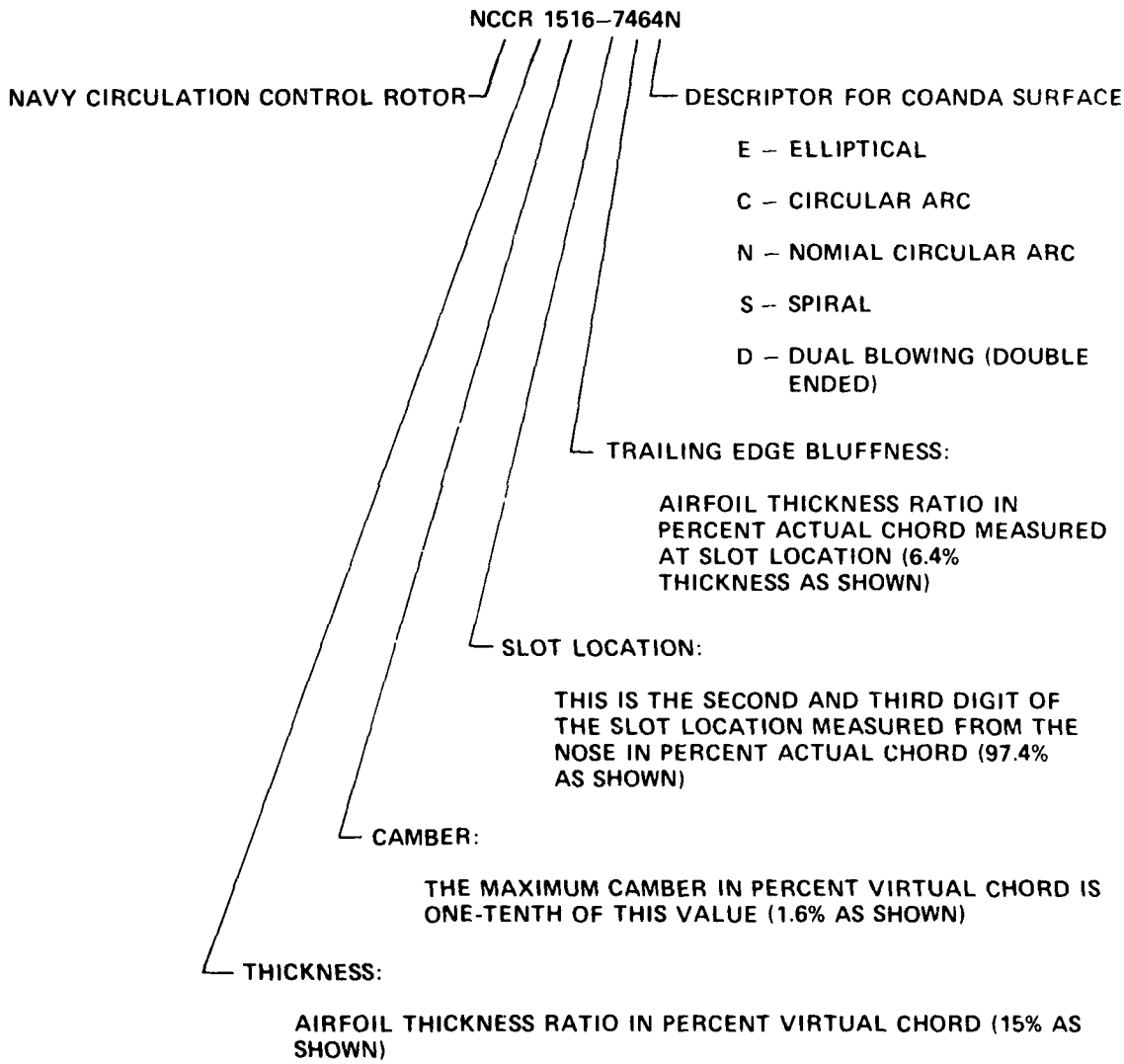

TABLE 2 - TWO-DIMENSIONAL MODEL COORDINATES FOR UPPER AND LOWER SURFACES

Upper Surface		Lower Surface	
X	Y	X	Y
0.0000	0.0000 Leading Edge	0.0000	0.0000 Leading Edge
-0.0111	0.0297	0.0114	-0.0177
-0.0075	0.1011	0.0182	-0.0259
0.0027	0.1283	0.0337	-0.0414
0.0280	0.1714	0.0613	-0.0626
0.0662	0.2159	0.1162	-0.0948
0.1601	0.2882	0.2206	-0.1478
0.4068	0.3892	0.359	-0.2111
0.8243	0.4902	0.4354	-0.2378
1.3058	0.5626	0.6313	-0.2890
1.7792	0.6118	0.8272	-0.3282
2.4723	0.6604	1.4815	-0.4128
3.0912	0.6872	2.2638	-0.4651
3.747	0.7016	3.0210	-0.4890
4.4168	0.7016	3.7529	-0.4966
5.2500	0.6779	4.4980	-0.4931
5.5430	0.6625	5.2207	-0.4803
5.9109	0.6367	6.0258	-0.4535
6.5054	0.5762	6.7567	-0.4091
7.0926	0.4823	7.2274	-0.3578
7.5185	0.3739	7.5127	-0.3065
7.6614	0.3217	7.6526	-0.2697
7.7332	0.2898	7.7449	-0.2378
7.8000	0.2549	7.821	-0.2038
7.84	0.2257	7.8955	-0.1589
7.892	0.1929	7.945	-0.1114
7.9169	0.1712	7.9648	-0.0918
7.9562	0.1279	7.9877	-0.0516
7.9914	0.0634	7.9947	-0.0311
8.0000	0.0000 Trailing Edge	8.0000	0.0000 Trailing Edge

DTNSRDC ISSUES THREE TYPES OF REPORTS

1. DTNSRDC REPORTS, A FORMAL SERIES, CONTAIN INFORMATION OF PERMANENT TECHNICAL VALUE. THEY CARRY A CONSECUTIVE NUMERICAL IDENTIFICATION REGARDLESS OF THEIR CLASSIFICATION OR THE ORIGINATING DEPARTMENT.

2. DEPARTMENTAL REPORTS, A SEMIFORMAL SERIES, CONTAIN INFORMATION OF A PRELIMINARY, TEMPORARY, OR PROPRIETARY NATURE OR OF LIMITED INTEREST OR SIGNIFICANCE. THEY CARRY A DEPARTMENTAL ALPHANUMERICAL IDENTIFICATION.

3. TECHNICAL MEMORANDA, AN INFORMAL SERIES, CONTAIN TECHNICAL DOCUMENTATION OF LIMITED USE AND INTEREST. THEY ARE PRIMARILY WORKING PAPERS INTENDED FOR INTERNAL USE. THEY CARRY AN IDENTIFYING NUMBER WHICH INDICATES THEIR TYPE AND THE NUMERICAL CODE OF THE ORIGINATING DEPARTMENT. ANY DISTRIBUTION OUTSIDE DTNSRDC MUST BE APPROVED BY THE HEAD OF THE ORIGINATING DEPARTMENT ON A CASE-BY-CASE BASIS.